**2023 Doctoral Thesis**

# The role of Paneth cell α-defensin as a regulator of the intestinal microbiota in nonalcoholic steatohepatitis

**(非アルコール性脂肪肝炎における腸内細菌叢の制御因子である Paneth 細胞α-defensin の役割)**

**Shunta Nakamura**

**Innate Immunity Laboratory**

**Graduate School of Life Science**

**Hokkaido University**

**September 2023**

**Table of contents**

**Chapter 1. General Introduction**

**Chapter 2. Materials and Methods**

2.1 Mice

2.2 Histological analysis

2.3 Reverse transcription and quantitative PCR

2.4 Fecal DNA extraction

2.5 16S rDNA sequencing

2.6 16S rDNA-based taxonomic analysis

2.7 Measurement of serum zonulin

2.8 Bacterial translocation

2.9 Quantification of fecal Crps

2.10 Whole-mount immunofluorescent staining and image analysis

2.11 Transmission electron microscopy

2.12 Paneth cell RNA-seq analysis

2.13 Visualization and quantification of Paneth cell granule secretion

2.14 Western blot analysis

2.15 Administration of R-Spo1 and Crp4

2.16 Data availability

2.17 Statistical analysis

**Chapter 3. Results**

3.1 Dysbiosis occurs before onset of NASH in CDAHFD-fed mice

3.2 Paneth cell α-defensin secretion decreases and relates to NASH dysbiosis

3.3 Restoration of α-defensin by R-Spo1 administration suppresses dysbiosis and prevents progression of NASH

3.4 Oral administration of α-defensin suppresses dysbiosis and ameliorates NASH pathology

**Chapter 4. Discussion**

4.1 Relationship between Paneth cell α-defensin and dysbiosis associated with NASH

4.2 Involvement of Paneth cell α-defensin in NASH pathology through regulation of the intestinal microbiota

4.3 Functional alterations of Paneth cell in NASH

4.4 The potential for prevention and treatment of NASH targeting Paneth cell α-defensin

**Chapter 5. Conclusion**

**References**

**Acknowledgements**

## Chapter 1. General Introduction

Nonalcoholic steatohepatitis (NASH) is a chronic liver disease characterized by steatosis, liver injury, inflammation, and fibrosis[1]. NASH is the crucial risk factor for cirrhosis and hepatocellular carcinoma and regarded as one of the urgent unmet medical needs with the rapidly increasing number of patients all over the world[2]. The liver fibrosis, which is a characteristic pathology of NASH, is associated with an increased risk for mortality, so that the prevention of fibrosis is important[3]. Obesity and type 2 diabetes are known to relate with NASH, and overnutrition is the principal cause of these disease[4]. Because the fibrosis progression rate among nonalcoholic fatty liver disease (NAFLD) patients is about 40% and NAFLD has a very variable natural history, a multiple hit hypothesis has been considered in which NASH development proceeds through the complex crosstalk of varied factors not limited to the liver[5,6,7]. The progression of NASH pathology is associated with overnutrition[8], yet the pathophysiological mechanisms of NASH are not well understood[9].

The human intestine harbors intestinal microbiota with 40 trillion bacteria, which affects health and disease via controlling host metabolism, immune function, and more[10,11]. On the other hand, dysbiosis, disruption of intestinal microbiota homeostasis, is associated with many diseases including metabolic disorders such as fatty liver and obesity[12,13]. The liver plays a central role in metabolism of the body and directly communicate with intestine to form the “gut-liver axis”, and the intestinal microbiota has a key role in the function of liver[14]. The metabolites, which are produced by the intestinal bacteria, such as secondary bile acids and short-chain fatty acids (SCFA) regulate liver fatty acid synthesis and bile acid synthesis[15,16]. Recently, the relationship between dysbiosis and NAFLD/NASH has been revealed. The composition of the intestinal microbiota in NASH patients is different from healthy individual[17]. Among NAFLD patients, differences in the intestinal microbiota have been reported between patients with NAFL and NASH as well as between severe and mild/moderate fibrosis[18,19]. Furthermore, alterations in the bacterial metabolites and influx of pathogen-associated molecular

patterns induce chronic inflammation in the liver[20,21]. These reports suggest that dysbiosis contributes to NASH progression.

A monolayer of the intestinal epithelium located at the interface between intestinal lumen and the lamina propria facilitates the absorption of nutrients and prevents the invasion of pathogen and more[22]. Paneth cells at the bottom of small intestinal crypts secrete granules rich in α-defensins, human defensin (HD) 5 in humans and cryptdins (Crps) in mice, into the intestinal lumen and contribute to innate enteric immunity by killing pathogenic bacteria[23,24,25,26,27]. Furthermore, α-defensin was shown to have selective bactericidal activities, killing pathogenic bacteria while eliciting less bactericidal activities against commensal bacteria[28]. Matrix metalloproteinase 7 (MMP7)-deficient mice absent of activated Crps increase the percentage of Firmicutes, in contrast, transgenic expression of HD5 decrease the percentage of Firmicutes[29,30]. In addition, MMP7 deficient mice impair symbiotic bacterial colonization after antibiotic treatment, indicating that α-defensin promotes commensal bacterial colonization under environmental stress[31]. These reports suggest Paneth cell α-defensin regulate the composition of the intestinal microbiota by selective bactericidal activity.

Paneth cell dysfunction has been reported to be associated with certain diseases. Deficiency in the autophagy gene *Atg16L1*, which has been identified as susceptible gene for Crohn's disease, leads to defects in granule secretion, as well as abnormal granule morphology and reduction of granule number[32]. In mouse model of allogeneic hematopoietic stem cell transplantation, graft-versus-host disease (GVHD) causes reduction of Paneth cells and α-defensins, that enhance bacterial translocation and further exacerbating the disease[33,34]. In contrast, restoration of luminal α-defensin prevented GVHD-mediated dysbiosis[35]. Furthermore, Paneth cell of severely obese patient showed abnormal granule morphology and decreased protein level of α-defensin[36], suggesting that dietary habits induce Paneth cell dysfunction. Taken together, these reports showed the possibility that impaired secretion of α-defensin from Paneth cell causes disease via dysbiosis[37].

In this study, we hypothesize that dietary factors composed with high fat triggers abnormalities in Paneth cell α-defensin to induce dysbiosis, resulting in NASH fibrosis. Here we show in diet-induced NASH model mice, the amount of α-defensin secreted from Paneth cells decreased significantly before the onset of NASH, resulting in dysbiosis with decreased microbiota diversity followed by fibrosis leading to NASH. Furthermore, restoring luminal amount of α-defensin by intravenous administration of R-Spondin1 (R-Spo1) that regenerates Paneth cells or oral administration of α-defensin both suppress dysbiosis and ameliorates liver fibrosis. Our results show for the first time that dysbiosis caused by decrease of Paneth cell α-defensin secretion in "gut-liver axis" contributes to the onset and the progression of NASH, further providing novel insights into Paneth cell α-defensin as a potential therapeutic target to contribute to prevention and treatment of NASH.

## Chapter 2. Materials and Methods

### 2.1 Mice

Three-week-old male C57BL/6J mice were purchased from CLEA Japan Inc. and acclimated for 3 weeks (wks) prior to be using in experiments. After acclimation, six-week-old mice were divided into two groups: SD group fed with standard diet (SD; A06071314, Research Diets Inc.) and CDAHFD group fed with choline-deficient, L-amino acid-defined, high-fat diet with 0.1% methionine (CDAHFD; A06071302, Research Diets Inc.). The mice were maintained on 12-h light/dark cycle and had free access to both food and tap water. All animal experiments in this study were conducted in accordance with the approval of the Institutional Animal Care and Use Committee of the National University Corporation at Hokkaido University in accordance with Hokkaido University Regulations of Animal Experimentation.

### 2.2 Histological analysis

The left lobe of liver was quickly excised and fixed in 10% neutral buffered formalin. 4 μm sections of paraffin-embedded tissue were stained using hematoxylin and eosin (H&E) or Sirius red. The average number of inflammatory foci and hepatocellular ballooning were determined from 5 randomly selected fields (228×303 $\mu m^2$) per slide by using image analysis software, NIS-Elements D ver. 4.13 (Nikon). Hepatocellular ballooning was scored as follow: 0 (ballooned cells are absent), 1 (ballooned cells are present). Using the BZ-II analyzer (KEYENCE), at least 20 fields (272×361 $\mu m^2$) per slide were quantified for lipid accumulation area and Sirius red-positive area, respectively, and the average percentage of hepatic steatosis area and fibrosis area were evaluated. TUNEL assay was performed using the apoptosis in situ detection kit (Wako) following manufacturer's instruction. TUNEL-positive cells were quantified by counting positive nuclei in 5 randomly selected fields (118×156 $\mu m^2$) per

slide by using NIS-Elements D.

### 2.3 Reverse transcription and quantitative PCR

DNA-free RNA was obtained from ileal or liver tissue by Dnase treatment using the RNeasy Mini Kit (QIAGEN). 0.5 μg total RNA was reverse transcribed with SuperScript VILO MasterMix (Life Technologies) by thermal cycled at 25 °C for 10 min, 42 °C for 60 min, and 85 °C for 5 min using Mastercycler EP (Eppendorf). Quantitative PCR was performed using Roche LightCycler 96 (Roche) with fluorescence-labeled locked nucleic acid (LNA) hydrolysis probes (Roche) from the Universal Probe Library (UPL) following the manufacturer's protocol. Gene expression was normalized to hypoxanthine guanine phosphoribosyl transferase-1 (Hprt1). The primer sequences are listed in Table 1.

Table 1 PCR primers

| Gene | Primer sequence (5'-3') | Universal Probe Library |
|---|---|---|
| *Pdia3* | F: TGGCCACTGTAAGAATCTGGA | #33 |
| | R: TGACAATATTTGGATCTTTGCTG | |
| *Perk* | F: CCTTGGTTTCATCTAGCCTCA | #106 |
| | R: ATCCAGGGAGGGGATGAT | |
| *Chop* | F: GCGACAGAGCCAGAATAACA | #91 |
| | R: GATGCACTTCCTTCTGGAACA | |
| *Nox2* | F: GATGCACTTCCTTCTGGAACA | #20 |
| | R: GTGCACAGCAAAGTGATTGG | |
| *Prdx6* | F: TTTCAATAGACAGTGTTGAGGATCA | #1 |
| | R: CCGTGGGTGTTTCACCAT | |
| *Atg3* | F: GTACCTGACCCCGGTCCT | #78 |
| | R: TTGGACAGTGGTGGACTAAGTG | |
| *Atg12* | F: CATTGACTTCATCAAAAAGTTCCTT | #49 |
| | R: GGCAAAGGACTGATTCACATAA | |
| *Lc3b* | F: CCCCACCAAGATCCCAGT | #7 |
| | R: CGCTCATGTTCACGTGGT | |
| *F4/80* | F: GGAGGACTTCTCCAAGCCTATT | #42 |
| | R: AGGCCTCTCAGACTTCTGCTT | |
| *Cd11b* | F: CAATAGCCAGCCTCAGTGC | #76 |
| | R: GAGCCCAGGGGAGAAGTG | |
| *Cd11c* | F: AGCCTCAAGACAGGACATCG | #106 |
| | R: TGAATCCTGGAGGGGATCT | |
| *Tgfb1* | F: CTGGGCACCATCCATGAC | #68 |
| | R: CAGTTCTTCTCTGTGGAGCTGA | |
| *Trailr2* | F: CCCTGAGATCTGCCAGTCAT | #103 |
| | R: TTTCTCTGGGGGTACAGGAA | |
| *Bax* | F: GAACCATCATGGGCTGGA | #69 |
| | R: GGTCCCGAAGTAGGAGAGGA | |
| *Crp1* | F: CCAAAACACAGATGAAGAGACTAAAA | #68 |
| | R: GCATACCAGATCTCTCAACGATT | |
| *HPRT-1* | F: TCCTCCTCAGACCGCTTTT | #95 |
| | R: CCTGGTTCATCATCATCGGCTAATC | |

### 2.4 Fecal DNA extraction

Fresh fecal samples were collected immediately after excretion, snap-frozen on dry ice, and stored at -80°C. For total DNA extraction, 200 mg fecal samples were treated with QIAamp Fast DNA Stool Mini Kit (QIAGEN) following the manufacturer's protocol. Final DNA concentrations were quantified from the absorption at 260 nm with a Nanodrop 2000 spectrometer (Thermo Fischer Scientific).

### 2.5 16S rDNA sequencing

The V3-V4 variable region of 16S ribosomal RNA genes were amplified from fecal DNA extracts using universal primer set of Bakt 341F (5-cctacgggnggcwgcag) and Bakt 805R (5-gactachvgggtatctaatcc)[38]. PCR amplification was performed with a 25 μL reaction volume mixtures comprising 0.5 ng/μL of DNA template, 200 nM of each primer and 1x KAPA HiFi Hot Start Ready Mix (Kapa Biosystems) under the conditions: initial denaturation at 95°C for 3 min, 25 cycles of 95°C for 30 sec, 55°C for 30 sec and 72°C for 30 sec, followed by final extension at 72°C for 5 min. Amplification products were then purified using AMPure XP beads (Beckman Coulter). Subsequently, index PCR was performed using a 50 μL reaction volume mixtures comprising 5 μL of purified PCR products, 5 μL of each index primer containing adapter sequence and sample specific 8 bp barcodes in the Nextera XT Index Kit v2 Set B (Illumina) and 1× KAPA HiFi Hot Start Ready Mix under the following conditions: 95°C for 3 min, 8 cycles of 95°C for 30 sec, 55°C for 30 sec and 72°C for 30 sec, followed by 72°C for 5 min. Resulting amplification products were purified using AMPure XP beads, quantified using the Qubit dsDNA HS Assay Kit (Invitrogen), and finally adjusted to 4 nM. Each amplicon was pooled and subjected to quantitative PCR using KAPA Library Quantification Kit Lightcycler 480 qPCR Mix (Kapa Biosystems), denatured following Illumina's guideline, and then adjusted to 4 pM. Amplicon library was combined with 5% of 4 pM PhiX Control v3 (Illumina) and

subjected to pair-end sequencing using MiSeq instrument with a MiSeq 600-cycle v3 kit (Illumina). Resulting sequence reads were filtered for read quality, basecalled, and demultiplexed using bcl2fastq software (Illumina).

### 2.6 16S rDNA-based taxonomic analysis

Taxonomic analysis of FASTQ files produced by MiSeq was conducted by QIIME2 software (version 2019.7)[39]. Quality-filtering, denoising, and removal of chimeric sequences were carried out by DADA2 plugin[40] using following parameters; --p-trim-left-f 17, --p-trim-left-r 21, --p-trunc-len-f 280, --p-trunc-len-r 200, --p-max-ee-f 2 –p-max-ee-r 2. Phylogenetic tree was constructed with FastTree[41] after alignment with MAFFT[42]. Each feature was classified by a naïve-bayes classifier based on 99% sequence identity to the SILVA database (v.132). α-Diversity (observed OTUs and Shannon index) and β-diversity (weighted UniFrac distance) were calculated by Qiime2 pipeline. Statistical significance of β-diversity was determined by PERMANOVA test in Qiime2 pipeline.

### 2.7 Measurement of serum zonulin

Serum zonulin levels were determined by Mouse Haptoglobin ELISA Kit (Abcam, ab157714). The assay was performed according to the manufacture's recommended methods.

### 2.8 Bacterial translocation

The spleen was removed and immediately placed into 500 μL of sterile Luria-Bertani (LB) medium too quantitate and identify bacteria. The spleen then was homogenized with a BioMasher (Nippi), and 200 μL was plated on LB agar plates and cultured either under aerobic conditions for 24 h or anaerobic conditions for 48 h at 37°C. Colony-forming unit (CFU) were counted and calculated per organ.

### 2.9 Quantification of fecal Crps

Fecal samples were dried and powdered by using a Multi-beads shocker (Yasui Kikai). 30 mg of fecal samples was vortex mixed in 300 μL PBS for 12 h at 4°C. The fecal suspension was centrifuged at 20,400 g for 10 min at 4°C, and Crp1 or Crp4 levels in supernatants were measured by sandwich ELISA as previously described[34,43].

### 2.10 Whole-mount immunofluorescent staining and image analysis

Whole-mount immunofluorescent staining was conducted using a modification of a previously reported method[44]. The ileal tissue was fixed in 4% paraformaldehyde (Sigma) for 2 h at room temperature. Fixed tissue was permeabilized with 0.5 % Triton X-100 (Sigma) overnight at room temperature, and then blocked with 10% goat serum (Sigma) and 0.5% Triton X-100 overnight at 4°C. For SD and CDAHFD group, antibody reaction was performed using FITC labeled mouse anti-Crp1 antibody (50 μg/mL, clone 77-R63, produced in our laboratory) and Alexa Fluor 647-labeled anti-mouse/human CD324 (E-cadherin) antibody (1:100, clone DECMA-1, BioLegend). For CDAHFD+PBS and CDAHFD+R-Spo1 group, the primary antibody reaction was performed with rabbit anti-Olfactomedin 4 (Olfm4) antibody (1:80, clone D6Y5A, Cell Signaling) for 1 day at 4°C, and then the secondary antibody reaction was performed with Alexa Fluor 555 conjugated F(ab′)2-goat anti-rabbit IgG (dilution 1:500, Thermo Fisher Scientific) and FITC labeled mouse anti-Crp1 antibody overnight at 4°C. Following washing, nuclei were stained with DAPI (Thermo Fisher Scientific). Samples were immersed in the optical-clearing solution (RapiClear 1.52, Sunjin Lab).

For quantification of Crp1 fluorescence intensity and counting numbers of Paneth cells and stem cells, Z-stack images were obtained using a confocal microscope (A1, Nikon) equipped with CFI Apo LWD 20X WI λS (Nikon). The number of Paneth cells was quantified by counting Crp1 immunostaining positive cells on 3 fields (150×150 $\mu m^2$) per tissue. The number of stem cells was quantified counting

Olfm4 positive cells on 3 fields (150×150 $\mu m^2$) per tissue. The region of interest was created using image analysis software, NIS-Elements AR ver. 5.11 (Nikon), and the Crp1 fluorescence intensity per Paneth cell was measured on 3 fields (150×150 $\mu m^2$) per tissue, and the mean intensity per field was calculated. For quantification of the number and diameter of Paneth cell granules, Z-stack images were obtained using A1 with CFI Apo TIRF 60X Oil (Nikon). The number and diameter of Paneth cell granules were measured on 3 fields (33×33 $\mu m^2$, 2 Paneth cells/field) per tissue.

**2.11 Transmission electron microscopy**

5-mm-long segments of terminal ileum were immediately fixed in 2% paraformaldehyde and 2% glutaraldehyde at 4°C for overnight. Then, samples were post-fixed with 2% osmium tetroxide at 4°C for 2 h. Dehydration was carried out, followed by embedding in Quetol-812 epoxy resin (Nisshin EM). After staining with 2% uranyl acetate and lead stain solution (Sigma), the ultrathin sections were examined with a JEM-1400Plus transmission electron microscope (JEOL Ltd.) at an acceleration voltage of 100 kV.

**2.12 Paneth cell RNA-seq analysis**

Crypts were isolated from the small intestine of mice fed with SD or CDAHFD for 3 wk as previously described[27]. In brief, the ileum segments were shaken in cold HBSS containing 30 mM EDTA. After vigorous shaking for ~300 times in HBSS, the isolated crypts were resuspended in HBSS containing 300 U/mL collagenase (Sigma), 10 mM Y-27632 (Sigma), and 1 mM N-acetylcysteine (Sigma), and shaken at 180 rpm for 5 min at 37 °C on a horizontal shaker (TAITEC). Then, 50 μg/μL Dnase I (Roche) was added, and the sample was mixed by pipetting. Cells were pelleted at 500 g for 5 min at 4°C and resuspended in washing buffer (DMEM/F12 containing 10 μM Y-27632 and 1 mM N-acetylcysteine), then passed through 40-μm cell strainer (BD Falcon). Paneth cells were stained with

Zinpyr-1 (Santa Cruz) and Allophycocyanin (APC) anti-CD24 (clone M1/69,)Abcam) in washing buffer for 10 min at 37°C. Following Paneth cell labeling, the cells were sorted by flow cytometry using a cell sorter (JSAN, Bay Bioscience). Single cells were gated by forward scatter and side scatter. Cells were sorted directly into lysis buffer for RNA isolation (PureLink RNA Mini Kit, Invitrogen). To make a pooled sample, at least 10,000 Paneth cells were sorted from 2 separate mice, and sorting experiment was repeated three times. 2 pools (each pool contains Paneth cells from 6 separate mice) were prepared for each group. Total RNA was isolated by Invitrogen® PureLink RNA Purification System according to manufacturer's instructions, and cDNA was synthesized using a SMART-Seq. Sequencing libraries were built with the TruSeq RNA Library Prep Kit (Illumina) and then submitted to Illumina NovaSeq 6000 for 100-bp PE reads sequencing. Fragments per kilobase of transcript per million mapped reads (FPKM) values were used, genes with FPKM values below 1 were not included in the analysis, and fold change ≥ 1.5 or ≤ 0.67 was considered differentially expressed.

**2.13 Visualization and quantification of Paneth cell granule secretion**

Paneth cell granule secretion was assessed by a modification of a previously reported method[27]. Isolated crypts from the distal 20 cm of small intestine of mice fed with SD and CDAHFD for 3 wk were embedded in Matrigel (Corning) on a collagen-coated 8 well chamber cover (Matsunami). After Matrigel polymerization, the enteroid culture media were added and incubated for 1 h at 37℃, 5% CO2. The enteroids were stimulated by 1 μM of carbamyl choline (CCh) (Sigma). The differential interference contrast images of Paneth cells before and 10 min after adding CCh were obtained from confocal microscopy (A1, Nikon). For quantification of Paneth cell granule secretion, area of the granules at pre-and post-stimulation was measured by using the image analysis software, NIS-Elements AR, and calculated percent granule secretion. Paneth cells in 10 crypts of each mouse (4 mice of each group) were evaluated.

### 2.14 Western blot analysis

Quantification of reduced-form Crp1 was performed as described previously[45]. In brief, 10 mg of freeze-dried powdered fecal samples were suspended with 100 µl of 30% (vol/vol) acetic acid and vortexed at 4°C overnight. Fecal suspension was centrifuged at 15,000 g for 30 min at 4°C. Supernatants were concentrated in a SpeedVac concentrator (Thermo Savant) and resuspended in 20 µl of PBS. 1 µL of resuspension was reacted with 9 µL of 20 ng/µL trypsin solution, and samples were subjected to Tris-Tricine SDS–PAGE. Proteins were transferred to polyvinylidene fluoride membranes. The membranes were blocked by BSA-free StabilGuard Immunoassay Stabilizer (Surmodics) and incubated with anti-Crp1 antibody (1 mg/mL, clone 76-R29, produced in our laboratory). The blots were visualized with Chemi-Lumi One ultra (Nacalai Tesque). For quantification of Crps, band intensities were determined by ImageJ software.

### 2.15 Administration of R-Spo1 and Crp4

Recombinant human R-Spo1 provided from Kyowa Kirin Co., Ltd was generated as previously reported[46,47]. R-Spo1 was intravenously administered at a dose of 600 µg three times a week for 3 wk. Recombinant Crp4, produced and purified as previously described[48], was orally administered at a dose of 110 µg twice daily for 6 wk.

### 2.16 Data availability

Paneth cell RNA-seq data were deposited in the NCBI's Sequence Read Archive (SRA PRJNA747067). 16S rRNA sequences were uploaded to the NCBI's SRA (PRJNA747068).

### 2.17 Statistical analyses

Data were analyzed with GraphPad Prism 8 software (Graphpad software), and results were represented as individual points with mean values and error bars representing SEM. Statistical significance between 2 groups was determined by unpaired two-tailed Student's t test. Pearson's test was used to analyze the correlation. A P value of less than 0.05 was considered statistically significant.

## Chapter 3. Results

### 3.1 Dysbiosis occurs before onset of NASH in CDAHFD-fed mice

Histological analyses of liver were conducted on mice fed standard diet (SD) or CDAHFD. At 1 wk, fat accumulation and inflammatory foci were observed in the CDAHFD group, also both the area of steatosis and the number of inflammatory foci increased with the number of wks on CDAHFD (Fig. 1, a and b). Hepatocellular ballooning increased at 3 wk in the CDAHFD group and continued to increase until 12 wk. Sirius red staining was performed to evaluate hepatic fibrosis, showing that Sirius red-positive fibrotic areas first appeared at 3 wk and continued to increase until 12 wk (Fig. 1, a and b). The number of TUNEL-positive liver cells in the CDAHFD group increased at 3 wk and continued to increase with NASH progression up to the 12 wk endpoint (Fig. 1c). These results showed that mice fed with CDAHFD developed progressive hepatic fibrosis with steatosis, lobular inflammation, and apoptosis, which reproduces the typical disease development of human NASH[9].

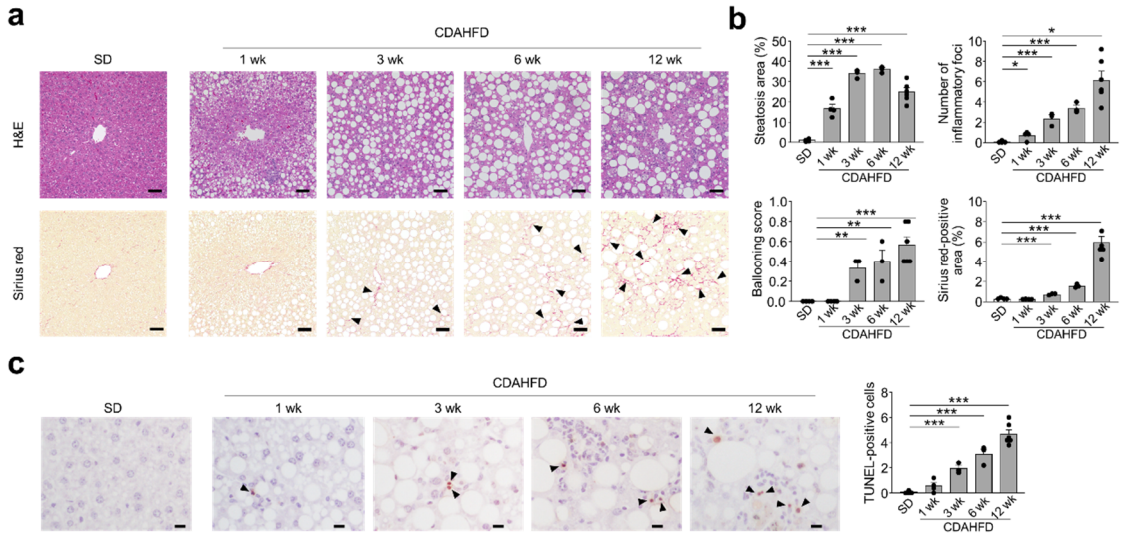


**Figure 1. Hepatic steatosis, lobular inflammation, hepatocellular ballooning, and fibrosis occur**

**in the CDAHFD group.**

(a) Representative images of H&E- and Sirius red-stained liver sections. Arrowheads indicate Sirius red-positive area. Scale bars: 50 μm. (b) Quantification of steatosis area, the number of inflammatory foci and Sirius red-positive area. (c) Representative images of TUNEL staining of liver sections (left). Arrowheads indicate TUNEL-positive cells. Scale bars: 10 μm. Quantification of TUNEL-positive cells (right). Data are shown as mean ± SEM for $n$ = 3–6 per group. *$P$ < 0.05, **$P$ < 0.01 and ***$P$ < 0.001, by unpaired 2-tailed Student's t test.

To examine whether endoplasmic reticulum (ER) stress, oxidative stress, and impaired autophagy, with known involvement in NASH pathology[7] occur in the CDAHFD group, specific marker gene expression was quantified by real-time PCR. Among ER stress markers, *Pdia3* mRNA levels decreased at 1 wk and increased at 3 wk, *Chop* mRNA levels increased at 6 and 12 wk, and *Perk* mRNA was elevated at 12 wk with CDAHFD feeding compared to the SD group (Fig. 2a). Expression of *Nox2* mRNA, a key source of redox radicals, increased, and levels of antioxidant enzyme *Prdx6* mRNA decreased, both after 1 wk of CDAHFD feeding (Fig. 2b). Among autophagy activating protein genes, *Atg3* mRNA declined after 1 wk on CDAHFD followed by decreasing levels of both *Atg12* and *Lc3b* mRNAs after 3 wk of CDAHFD feeding (Fig. 2c). In addition, *F4/80* and *Cd11b*, markers of resident and invasive macrophages, respectively, and dendritic cell marker *Cd11c* mRNA levels continued to increase after 1 wk (Fig. 2d). Fibrosis related growth factor *Tgfb1* continued to increase after 3 wk of CDAHFD feeding. mRNA levels for *Trailr2* increased from 1 wk, and *Bax* mRNA levels were elevated at 12 wk in the CDAHFD group (Fig. 2e). These results showed that inflammation and apoptosis in the liver contributed to the onset and progression of fibrosis and that ER stress, oxidative stress, and impairment of autophagy were involved in NASH development of the CDAHFD group.

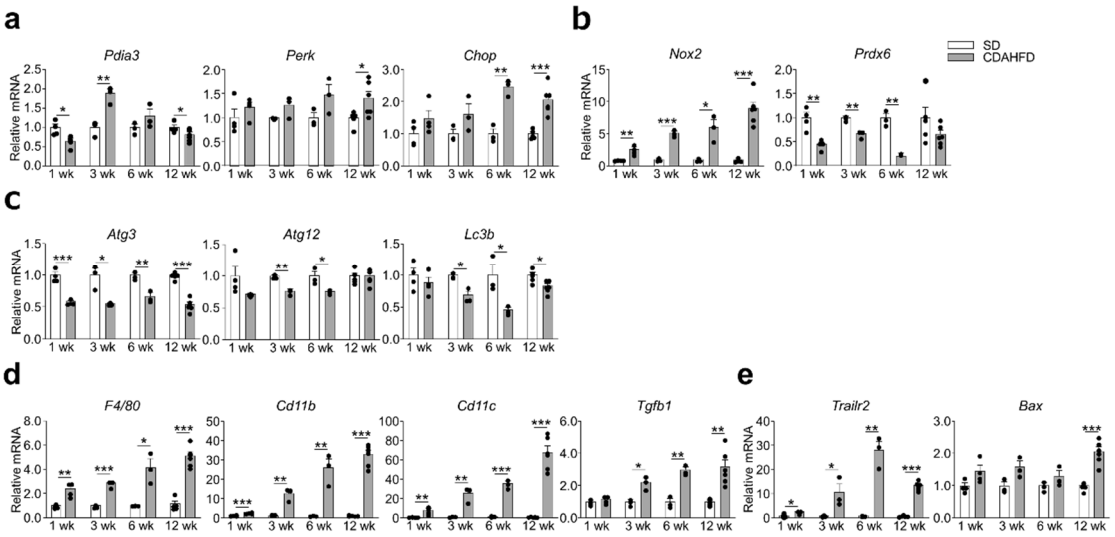


**Figure 2. The CDAHFD group develops NASH pathology associated with dysregulated expression of ER stress, oxidative stress, and autophagy related genes.**

(a–e) Hepatic mRNA expression of ER stress (a), oxidative stress (b), autophagy (c), inflammation (d), and apoptosis related genes (e) was analyzed by real-time PCR. Data are shown as mean ± SEM for $n$ = 3–6 per group. *$P < 0.05$, **$P < 0.01$ and ***$P < 0.001$, by unpaired 2-tailed Student's t test.

To investigate whether dysbiosis occurs in the CDAHFD group, we conducted 16S rRNA gene sequencing on fecal DNA. α-Diversity analysis showed that observed both operational taxonomic units (OTUs) and Shannon index were significantly decreased in the CDAHFD group from 1 wk (Fig. 3a). Principal coordinates analysis (PCoA) showed that the composition of intestinal microbiota in the CDAHFD group was different from that of the SD group after 1 wk and continued through 12 wk (Fig. 3b). At the family level, the relative abundances of Eggerthellaceae, Bacteroidaceae, Prevotellaceae, Streptococcaceae, Peptostreptococcaceae, and Ruminococcaceae were significantly increased in the CDAHFD group. In contrast, Muribaculaceae, unassigned family of unassigned Bacteroidia class,

unassigned Clostridiales, Clostridiales VadinBB60 group, and Erysipelotrichaceae were significantly decreased relative to the SD group (Fig. 3c). At the genus level, a total of 18 genera showed significantly increased after CDAHFD feeding while total of 10 genera decreased in the CDAHFD group during disease progression (Fig. 3d). These results showed that dysbiosis occurs before the onset of NASH in mice fed CDAHFD.

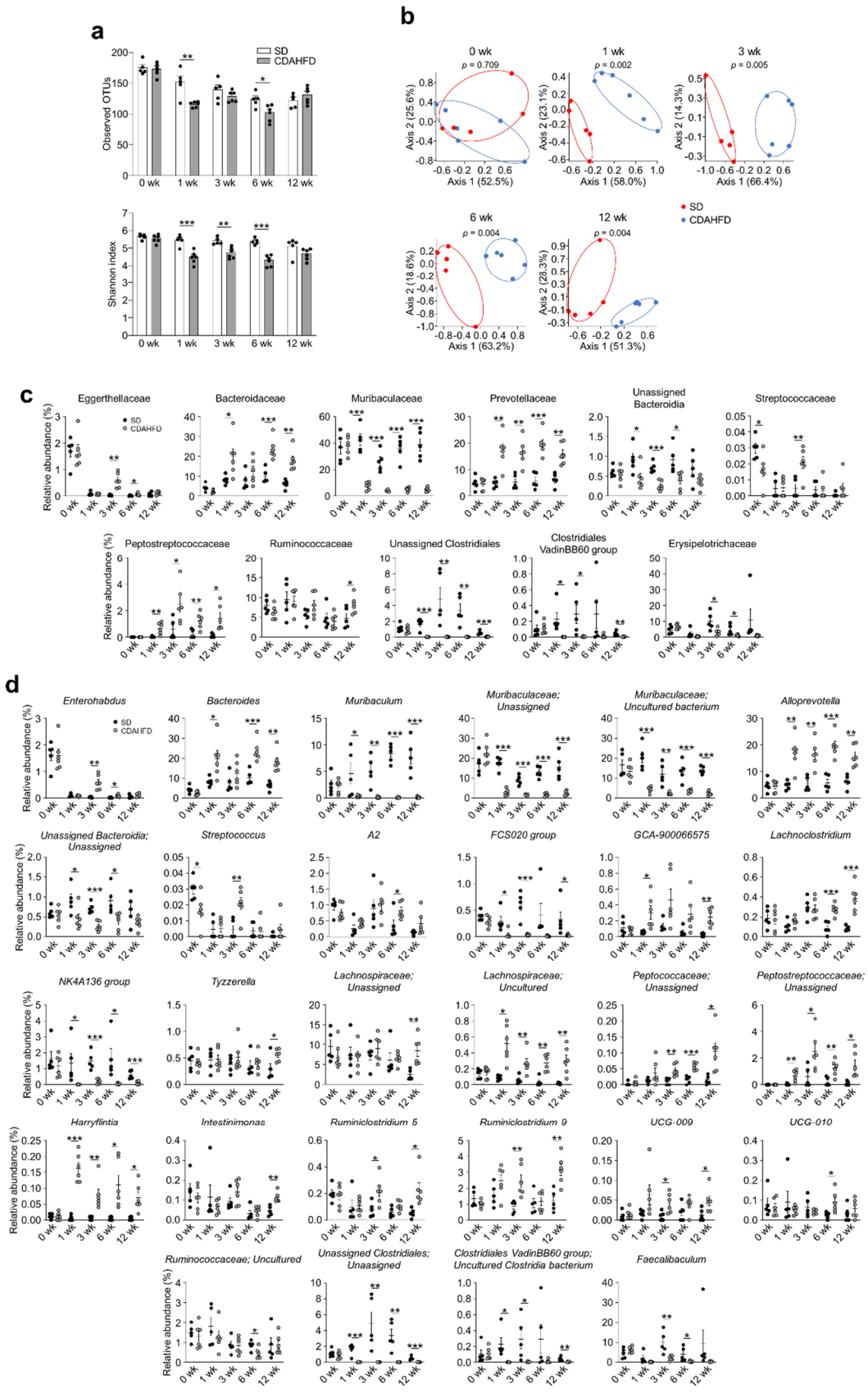
a
Observed OTUs
SD
CDAHFD
0 wk
1 wk
3 wk
6 wk
12 wk
Shannon index
b
0 wk
p = 0.709
1 wk
p = 0.002
3 wk
p = 0.005
6 wk
p = 0.004
12 wk
p = 0.004
Axis 1 (52.5%)
Axis 2 (25.6%)
Axis 1 (58.0%)
Axis 2 (23.1%)
Axis 1 (66.4%)
Axis 2 (14.3%)
Axis 1 (63.2%)
Axis 2 (18.6%)
Axis 1 (51.3%)
Axis 2 (28.3%)
c
Eggerthellaceae
Bacteroidaceae
Muribaculaceae
Prevotellaceae
Unassigned Bacteroidia
Streptococcaceae
Peptostreptococcaceae
Ruminococcaceae
Unassigned Clostridiales
Clostridiales VadinBB60 group
Erysipelotrichaceae
Relative abundance (%)
d
Enterohabdus
Bacteroides
Muribaculum
Muribaculaceae; Unassigned
Muribaculaceae; Uncultured bacterium
Alloprevotella
Unassigned Bacteroidia; Unassigned
Streptococcus
A2
FCS020 group
GCA-900066575
Lachnoclostridium
NK4A136 group
Tyzzerella
Lachnospiraceae; Unassigned
Lachnospiraceae; Uncultured
Peptococcaceae; Unassigned
Peptostreptococcaceae; Unassigned
Harryflintia
Intestinimonas
Ruminiclostridium 5
Ruminiclostridium 9
UCG-009
UCG-010
Ruminococcaceae; Uncultured
Unassigned Clostridiales; Unaasigned
Clostridiales VadinBB60 group; Uncultured Clostridia bacterium
Faecalibaculum
Relative abundance (%)

**Figure 3. Dysbiosis occurs before onset of NASH in the CDAHFD group.**

(a) Observed OTUs and Shannon index in SD and CDAHFD groups. (b) PCoA plot of intestinal microbiota based on weighted UniFrac distance of SD and CDAHFD groups. (c, d) Relative abundance of individual genera that were significantly different between the SD and CDAHFD groups at the family (c) and genus level (d). Data are shown as mean ± SEM for $n$ = 5–6 per group. The data represent mean ± SEM. *$P$ < 0.05, **$P$ < 0.01 and ***$P$ < 0.001, by unpaired 2-tailed Student's t test.

Because increased intestinal permeability associated with dysbiosis contributes to NASH progression via the influx of intestinal bacteria and bacterial components into the liver, we next measured serum zonulin, a marker of intestinal permeability[49]. At 1 wk, the SD and CDAHFD groups had similar serum zonulin levels. However, at 3 wk and continuing for 12 wk, serum zonulin levels in the CDAHFD group were increased significantly compared to the SD group sera (Fig. 4a). We further investigated whether bacterial translocation occurred. Bacterial colonies were detected in the spleen at 6 wk in the CDAHFD group (Fig. 4b). These results indicated that intestinal hyperpermeability accompanied by dysbiosis occurred in the CDAHFD group.

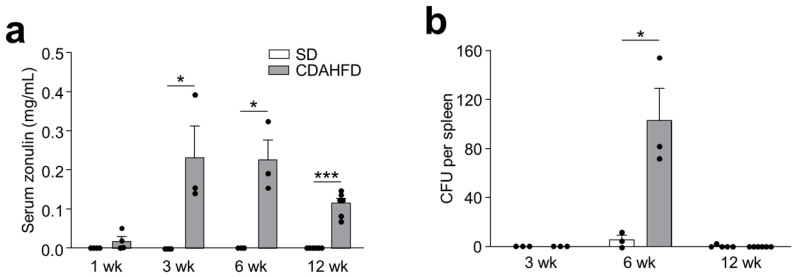


**Figure 4. Increased intestinal permeability and bacterial translocation to spleen occurs in the CDAHFD group.**

(a) Serum zonulin levels in SD and CDAHFD group. (b) Quantification of bacteria in spleen by CFUs cultured from spleen of SD and CDAHFD group at 3, 6, and 12 wk under anaerobic condition. Data are shown as mean ± SEM for $n$ = 3–6 per group. The data represent mean ± SEM. *$P$ < 0.05, **$P$ < 0.01 and ***$P$ < 0.001, by unpaired 2-tailed Student's t test

### 3.2 Paneth cell α-defensin secretion decreases and relates to NASH dysbiosis

Because Paneth cell α-defensin have a role as regulator of the intestinal microbiota, we next examined whether Paneth cell α-defensins are involved in the onset of NASH in the CDAHFA group. To evaluate the quantity of α-defensins secreted by Paneth cells, fecal levels of Crp1, one of the most abundant Crps in the small intestine[50], were measured. Before the onset of liver fibrosis, Crp1 secretion in the CDAHFD group significantly decreased compared to the SD group and continued for 12 wk (Fig. 5).

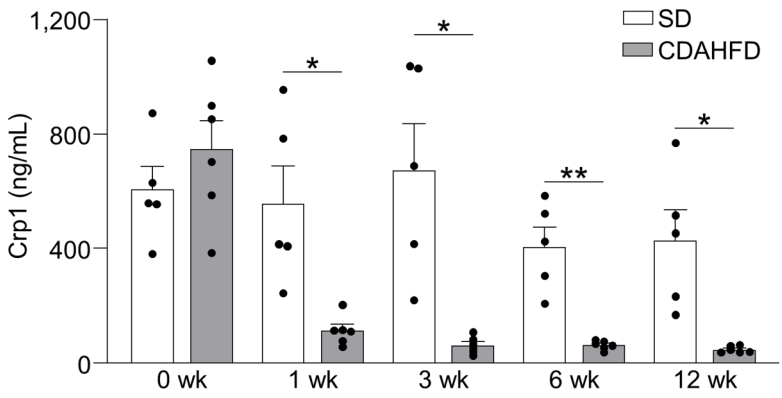


**Figure 5. Secretion of Paneth cell α-defensin decrease in the CDAHFD group.**

Quantification of fecal levels of Crp1. Data are shown as mean ± SEM for $n$ = 5–6 mice/group. *$P$ <

0.05 and $^{**}P < 0.01$, by unpaired 2-tailed Student's t test.

To determine whether decreased α-defensin secretion is associated with dysbiosis and NASH pathogenesis, correlation analyses among quantity of α-defensin levels in feces, the abundance of the intestinal microbiota, and NASH pathology were conducted. Among 28 genera at the genus level, which showed significantly different proportion between the SD and CDAHFD groups during disease progression (Fig. 3d), twenty genera showed a positive or negative correlation with fecal Crp1 (Fig. 6). Among them, the relative abundance of 10 genera which increased in the CDAHFD group, including *Bacteroides*, *Alloprevotella*, *GCA-900066575*, *Lachnoclostridium*, uncultured Lachnospiraceae, unassigned Peptostreptococcaceae, *Harryflintia*, *Ruminiclostridium 5*, *Ruminiclostridium 9*, and *UCG-009*, correlated positively with NASH pathology including steatosis, inflammation, apoptosis, and fibrosis. On the other hand, the 6 genera that decreased in abundance, i.e., *Muribaculum*, unassigned Muribacululaceae, Muribaculaceae uncultured bacterium, *NK4A136 group*, unassigned genus of the unassigned Clostridiales family, and uncultured Clostridiales VadinBB60 group, correlated negatively (Fig. 6). Our results identified total 16 genera which related

with both Crp1 reduction and NASH pathophysiology, suggesting that Crp1 reduction contributed to NASH progression via alterations in these intestinal bacteria.

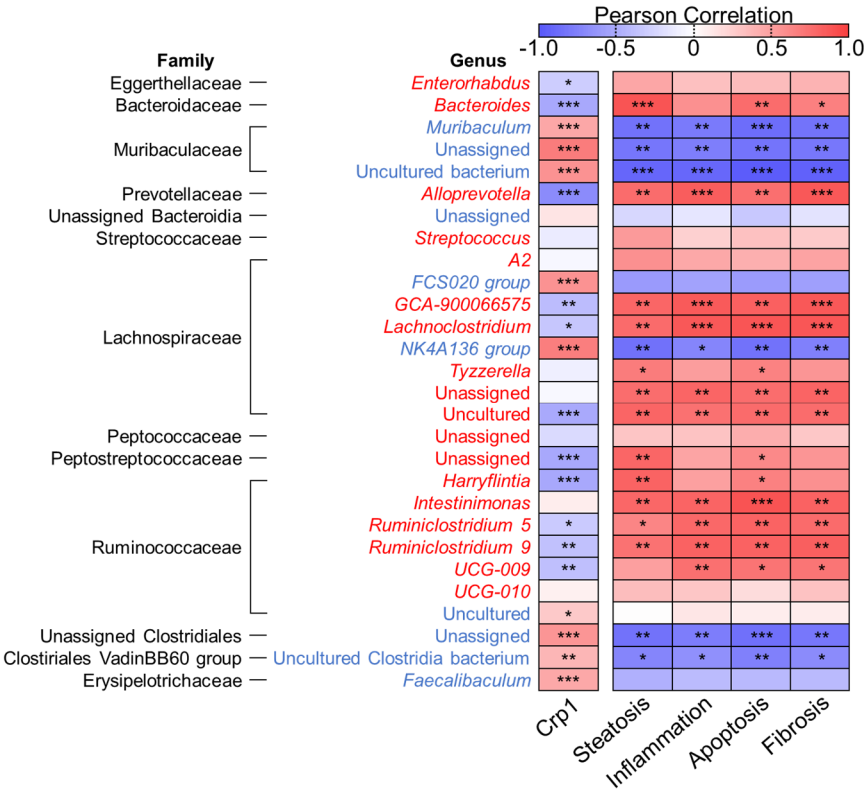


**Figure 6. The CDAHFD group shows dysbiosis correlated with both the quantity of fecal α-defensin and NASH pathology.**

28 genera that were significantly increased or decreased in CDAHFD group compared with SD group. Red indicates genera significantly increased in CDAHFD group, and blue indicates genera significantly decreased in CDAHFD group. Heatmap showing Pearson correlation coefficients between relative abundance of significantly changed genera in CDAHFD group and fecal Crp1 levels from Fig. 5 or NASH pathology from Fig. 1b. Correlation analysis between Crp1 levels and relative abundance of individual genera was conducted using the data of 1, 3, 6, and 12 wk. Correlation analysis between NASH pathology and relative abundance of individual genera was conducted using

the data of 12 wk. *$P$ < 0.05, **$P$ < 0.01 and ***$P$ < 0.001, by Pearson correlation test.

To investigate the cause of decreased Crp1 secretion, Crp1 mRNA expression, Paneth cell number, and whole-mount fluorescence immunostaining of Crp1 were performed on the ileal tissue samples. For both Crp1 mRNA expression and Paneth cell number, no differences were observed between the SD and CDAHFD groups (Fig. 7, a–d). In contrast, fluorescent intensities of Crp1 in the CDAHFD group were diminished compared to the SD group after 3 wk (Fig. 7, c and e), indicating protein expression of α-defensin decreased in Paneth cells of the CDAHFD group.

Because α-defensins are abundant in Paneth cell granules under normal conditions, we examined the morphology of Paneth cell granules to possibly explain the decreased levels of α-defensins in Paneth cells of the CDAHFD group. The diameter of Paneth cell granules decreased after 1 wk of the CDAHFD group, and the numbers of Paneth cell granules also decreased from 3 to 12 wk (Fig. 7, f–h). Transmission electron microscopy images confirmed the abnormal morphologies of Paneth cell granules in the CDAHFD group (Fig. 7i).

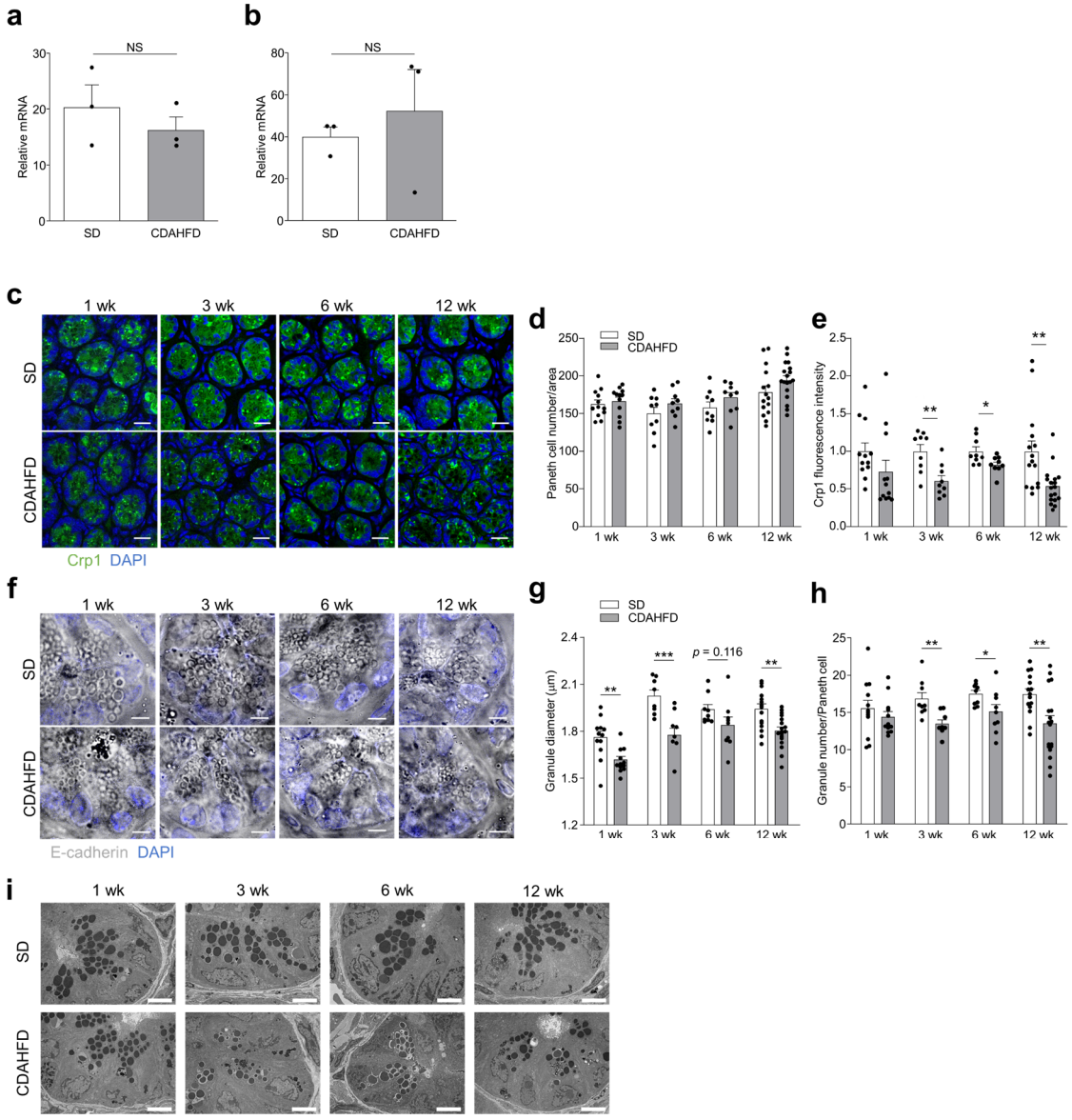


**Figure 7. Paneth cells of the CDAHFD group showed decreased protein expression of α-defensin and abnormal granules.**

(a, b) mRNA levels of Crp1 in ileum of SD and CDAHFD group at 3 wk (a), and 6 wk (b) analyzed by real time-PCR. Data are shown as mean ± SEM for *n* = 3 mice/group. (c) Representative images of immunofluorescence staining of Crp1 (green) in small intestine from SD and CDAHFD group. DAPI (blue) stains the nucleus. Scale bars: 20 μm. (d, e) Quantification of the number of Paneth cells (d) and Crp1 fluorescence intensity on Paneth cells (e) shown in c. Data are shown as mean ± SEM for *n*

= 9–18 fields/group and quantified based on 3 fields per mouse. (f) Representative images of whole mount small intestine obtained with confocal microscopy. Scale bar: 5 μm. (g, h) Granule diameter (g) and granule number (h) of each Paneth cell per field shown in f. Data are shown as mean ± SEM for $n$ = 9–18 fields/group and quantified based on at least 3 fields per mouse. Each group contains 3–6 mice. (i) Representative images of transmission electron microscopy of Paneth cells at the base of the ileal crypts in SD and CDAHFD group at 1, 3, 6, and 12 wk. Paneth cells in SD group have tightly packed electron-dense core granules, in contrast, Paneth cells in CDAHFD group have fewer loosely packed granules with a halo appearance. $n$ = 1 for each group. Scale bars: 5 μm. (a, b, d, e, g, h) *$P$ < 0.05, **$P$ < 0.01 and ***$P$ < 0.001, by unpaired 2-tailed Student's t test. NS, not significant.

To further determine the molecular basis for these functional alterations in Paneth cells, RNA sequencing (RNA-seq) analysis was performed on isolated small intestinal Paneth cells from the SD and CDAHFD groups. One hundred and forty-five genes were upregulated in CDAHFD mice compared to the SD group, while 2,202 genes were downregulated in the CDAHFD group (Fig. 8a). These differentially regulated genes were compared with gene products by referring to GO terms: Secretion (GO: 0046903) and trans-Golgi network (GO: 0005802), known to be important in the granule secretory pathway. Twelve upregulated genes in CDAHFD Paneth cells include ion transporter *Car4*, oxidative stress gene *Chac1*, glycosylation protein *Tmem165*, and secretion protein *Stxbp1*. The 97 down regulated genes include ion transporters *Cacr2a*, *Kcnq1*, *Cftr*, and *Kcnn4*, vesicle transporters *Optn*, *Trappc9*, *Vamp2*, *Dop1a*, *Rab26*, *Lrba*, *Arfrp1*, and *Gga3*, autophagy related proteins *Klhl20*, *Nlrp6*, *Ap4m1*, and *Bsn*, and oxidative stress related protein *Arntl1* (Fig. 8b). These results indicated that expression of genes related to the granule secretory pathway, including vesicle transporters and ion channel transporters, is dysregulated in Paneth cells of the CDAHFD group. Thus, to evaluate

Paneth cell granule secretion of the CDAHFD group directly, granule secretory responses of Paneth cells were visualized in enteroids, a three-dimensional culture system of small intestinal epithelial cells[27]. When CCh, which induces Paneth cell granule secretion, was added to enteroid cultures derived from small intestinal crypts of the CDAHFD group, the quantity of granules secreted by Paneth cells was significantly lower than that of SD group enteroids (Fig. 8c). These results revealed that Paneth cells in the CDAHFD group decreased α-defensin secretion into the intestinal lumen due to decreased protein expression of α-defensin and impaired granule secretory function.

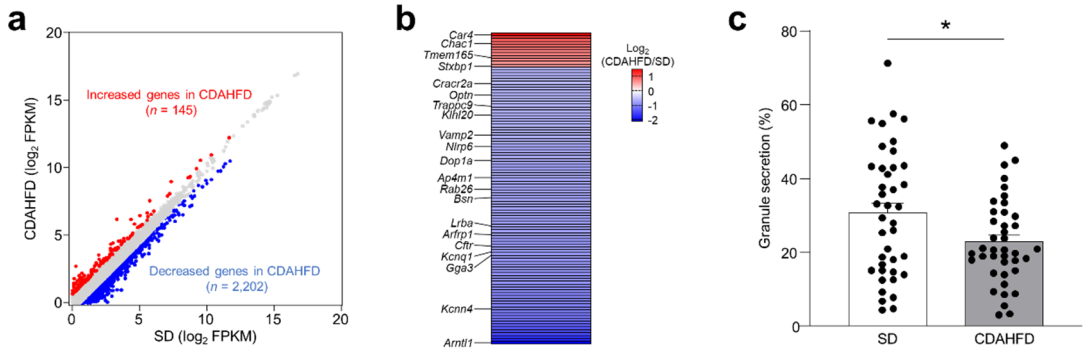


**Figure 8. Paneth cell granule secretion is impaired in the CDAHFD group.**

(a) Scatterplot of global gene expression profiles of SD and CDAHFD group derived from RNA-seq analysis. (b) Heatmap showing log2 fold change of differentially expressed genes (1.5-fold increase or decrease) associated with Paneth cell functions in CDAHFD group compared with SD group. (c) Enteroids derived from the small intestine of SD and CDAHFD groups were stimulated by 1 mM CCh for 10 min. Percent granule secretion was calculated as percent area granule secretion. Data are shown as mean ± SEM for $n = 40$ crypts/group. Each group contains 4 mice. *$P < 0.05$, by unpaired 2-tailed Student's t test.

It has been reported that abnormal Paneth cells secrete reduced-form α-defensin that lack disulfide bonds resulting in disruption the spectrum of bactericidal activity and are involved in the development of ileitis via dysbiosis in Crohn's disease model mice[45]. Therefore, we further measured the amount of reduced-form Crp1 (rCrp1) in feces of the CDAHFD group. Oxidized-form crp1 (oxCrp1) decreased in the CDAHFD group compared to the SD group, whereas rCrp1 was not detected in both at 3 and 12 wk (Fig. 9, a and b). These results indicated that Paneth cell dysfunction impairs granule secretion, resulting in diminished release of native, i.e., oxidized-form, α-defensins into the intestinal lumen.

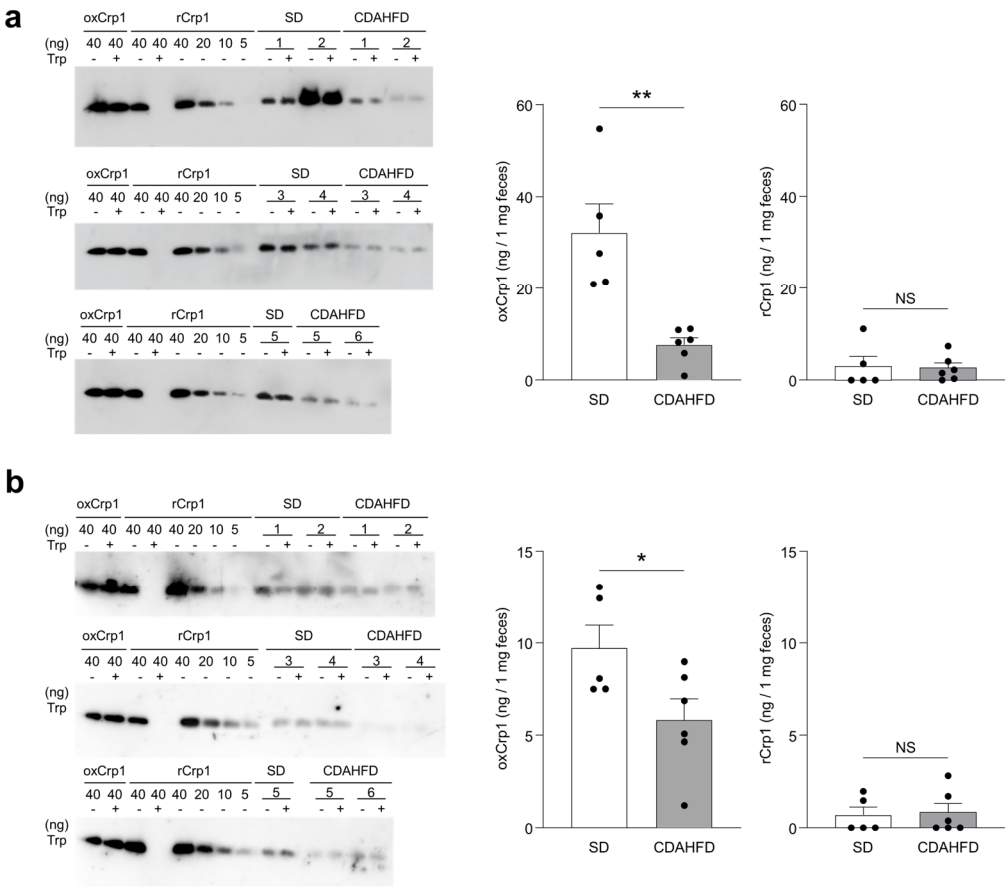


**Figure 9. Paneth cells in the CDAHFD group do not secrete reduced-form α-defensins.**

Tricine SDS-PAGE Western blot analysis of oxCrp1 or rCrp1 in fecal extracts of SD and CDAHFD

group at 3 wk (a) and 12 wk (b). Chemically synthesized ox and rCrp1 were used as positive controls. Each sample was treated with trypsin (Trp+) or PBS (Trp−). Crps detected in Trp− were considered to be the sum of ox and rCrp1, and Crps detected in Trp+ were considered as rCrp1 that escaped tryptic digestion. The amount of ox and rCrp1 in fecal extracts. The amount of oxCrp1 in each sample was calculated from band intensity of Trp+, and the amount of rCrp1 was calculated from the difference between band intensity of Trp− and Trp+. Data are shown as mean ± SEM for $n$ = 5–6 per group. The data represent mean ± SEM. *$P$ < 0.05 and **$P$ < 0.01 by unpaired 2-tailed Student's t test. NS, not significant.

### 3.3 Restoration of α-defensin by R-Spo1 administration suppresses dysbiosis and prevents progression of NASH

To clarify the association between the early reduction of secreted luminal Paneth cell α-defensins and dysbiosis along with NASH progression, we tested whether restoration of α-defensins prevented dysbiosis induced by CDAHFD feeding. Because Wnt activator R-Spo1 enhances α-defensin secretion by stimulating enhanced Paneth cell differentiation from stem cells[35], CDAHFD-fed mice were injected intravenously with R-Spo1 for 3 wk. Measurements of fecal Crp1 tested whether R-Spo1 treatment restored luminal levels of secreted Crp1. Fecal Crp1 levels in the R-Spo1-treated CDAHFD mice (CDAHFD+R-Spo1 group) were increased at 1 wk, and after 2 wk, significantly increased compared to CDAHFD-fed mice treated with PBS (CDAHFD+PBS group) (Fig. 10a). Paneth cell numbers in CDAHFD+R-Spo1 mice were increased significantly at 3 wk along with stem cells, showing that R-Spo1 treatment restored luminal Crp1 levels by elevating Paneth cell numbers

(Fig. 10b).

Next, we assessed whether enhanced luminal Crp1 levels by R-Spo1 treatment attenuates dysbiosis. Among the families of intestinal bacteria which increased in mice fed CDAHFD during disease progression (Fig. 3c), the relative abundances of Prevotellaceae and Peptostreptococcaceae were reduced by R-Spo1 treatment. In contrast, R-Spo1 treatment decreased the proportion of enteric microbiota that showed increases during disease progression, including Muribaculaceae, unassigned Clostridiales, and unassigned family of unassigned Bacteroidia (Fig. 10c). Fecal Crp1 levels were positively correlated with the relative abundance of Muribaculacea and unassigned Clostridiales (Fig. 10c). At the genus level, among the intestinal bacteria that correlated with both fecal Crp1 levels and NASH pathology (Fig. 3d), the proportion of *Muribaculum*, unassigned Muribaculaceae, Muribaculaceae uncultured bacterium, and unassigned Clostridiales was restored by R-Spo1 treatment, showing positive correlation with Crp1 levels. Also, the outgrowth of *Harryflintia* was inhibited, showing negative correlation with Crp1 levels (Fig. 10d). These results indicated restoration of luminal α-defensin by R-Spo1 administration suppressed dysbiosis related to NASH.

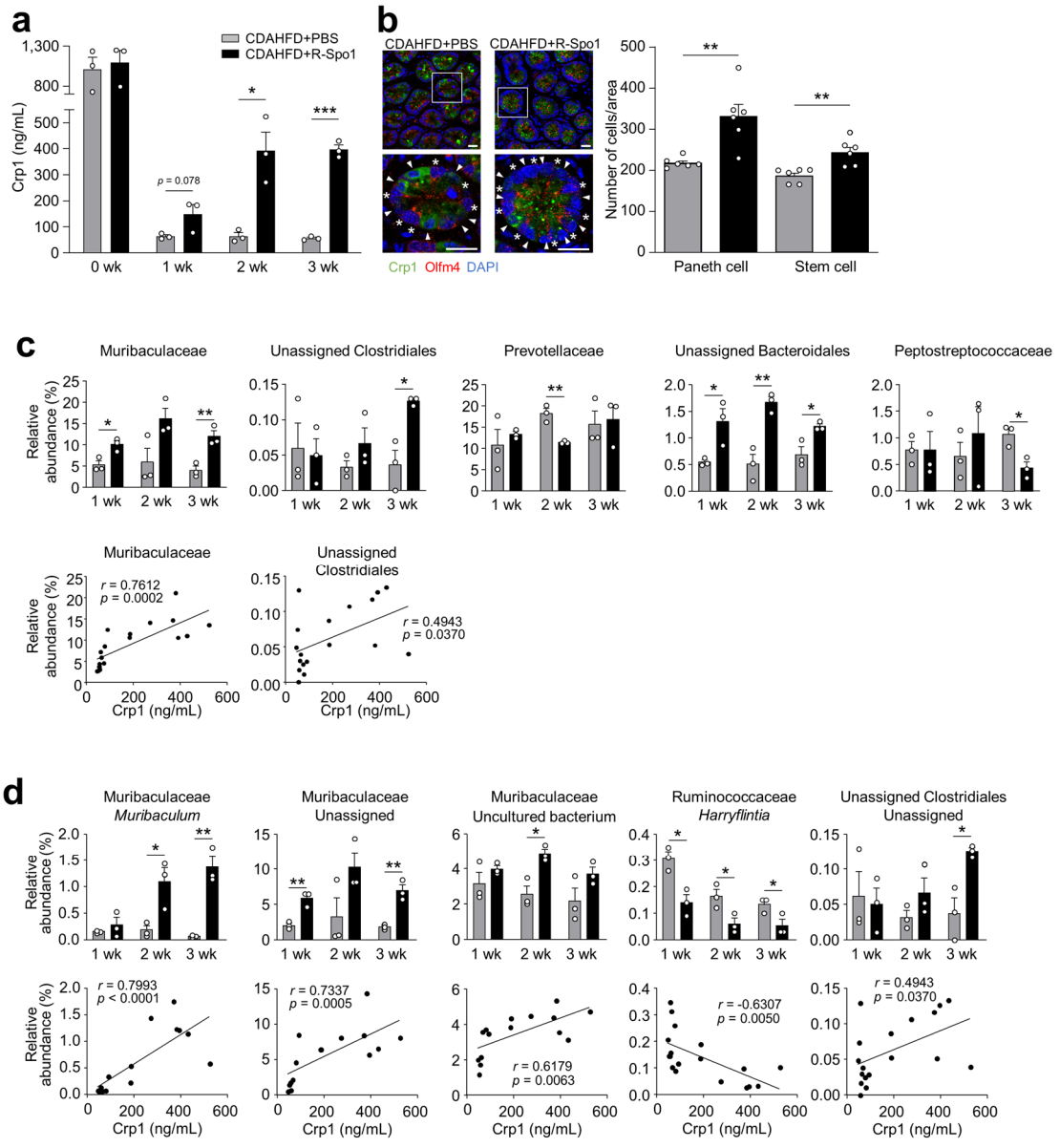


**Figure 10. R-Spo1 restores luminal α-defensin and suppresses dysbiosis.**

Six-week-old C57BL/6J mice were fed CDAHFD to induce NASH and intravenously injected with R-Spo1 at a dose of 600 μg or PBS three times a week for 3 wk. (a) Fecal Crp1 levels in the CDAHFD+PBS and CDAHFD+R-Spo1 groups. (b) Representative images of immunofluorescence staining of Crp1 (green) and Olfm4 (red) in small intestine from CDAHFD+PBS and CDAHFD+R-Spo1 mice at 3 wk (left). Arrowheads indicate Paneth cells and asterisk indicate stem cells. Scale bar:

20 μm. Quantification of the number of Paneth cells assessed by expression of Crp1 and the number of stem cells assessed by expression of Olfm4 per ileal unit area (right). Data are shown as mean ± SEM for $n$ = 6 fields/group and quantified based on at least 2 fields per mouse. Each group contains 3 mice. (c) Relative abundance of individual genera that were significantly recovered in CDAHFD+R-Spo1 group from CDAHFD mice of 11 family in Fig. 3c (upper panel). Correlation analysis between fecal Crp1 levels and relative abundance of individual genera CDAHFD+PBS and CDAHFD+R-Spo1 group (lower panel). (d)Relative abundance of individual genera that were significantly recovered in CDAHFD+R-Spo1 group from CDAHFD group of 28 genera shown in Fig. 3d (upper panel). Correlation analysis between fecal Crp1 levels and relative abundance of individual genera (lower panel). $r$ and $P$ values by Pearson correlation test are presented. Data are shown as mean ± SEM for $n$ = 3 per group. *$P$ < 0.05, **$P$ < 0.01 and ***$P$ < 0.001, by unpaired 2-tailed Student's t test.

To discern the suppression of dysbiosis due to restoration of α-defensin by R-Spo1 administration prevented NASH development, histological analysis of liver was conducted. The area of steatosis, the numbers of inflammatory foci, hepatocellular ballooning, and the area of fibrosis all were decreased significantly in the CDAHFD+R-Spo1 group compared to the CDAHFD+PBS group (Figure 11, a and b). R-Spo1 treatment significantly decreased hepatic mRNA levels of *Nox2*, *F4/80*, *Tgfb1*, *Trailr2*, and *Bax*, tended to decrease *Cd11c* expression, and decreased the number of TUNEL-positive cells significantly (Fig. 11, c and d). These results indicated that R-Spo1 treatment attenuated steatosis, inflammation, apoptosis, and fibrosis in the livers of mice fed CDAHFD. Among the genus of intestinal bacteria corrected for abnormal occupancy by R-Spo1 treatment (Fig. 10d), both *Muribaculum* and unassigned Muribaculaceae showed negative correlation with the steatosis area, the number of TUNEL-positive cells, and the area of fibrosis, and unassigned genus of the unassigned

Clostridiales family was negatively correlated with numbers of TUNEL-positive cells (Fig. 11e). The number of inflammatory foci was negatively correlated with Muribaculaceae uncultured bacterium, positively correlated with *Harryflintia*, and tended to be negatively correlated with *Muribaculum*, Muribaculaceae uncultured bacterium and unassigned genus of the unassigned Clostridiales family (Fig. 11e). In addition, fecal Crp1 levels were negatively correlated with the number of inflammatory foci, the number of TUNEL-positive cells, and the fibrosis area, indicating restoration of Crp1 secretion ameliorated NASH pathology (Fig. 11f). Taken together, these results indicated that enhancing luminal α-defensin secretion from Paneth cells by R-Spo1 treatment reduces liver fibrosis via ameliorating inflammation and apoptosis in the liver along with suppressing dysbiosis.

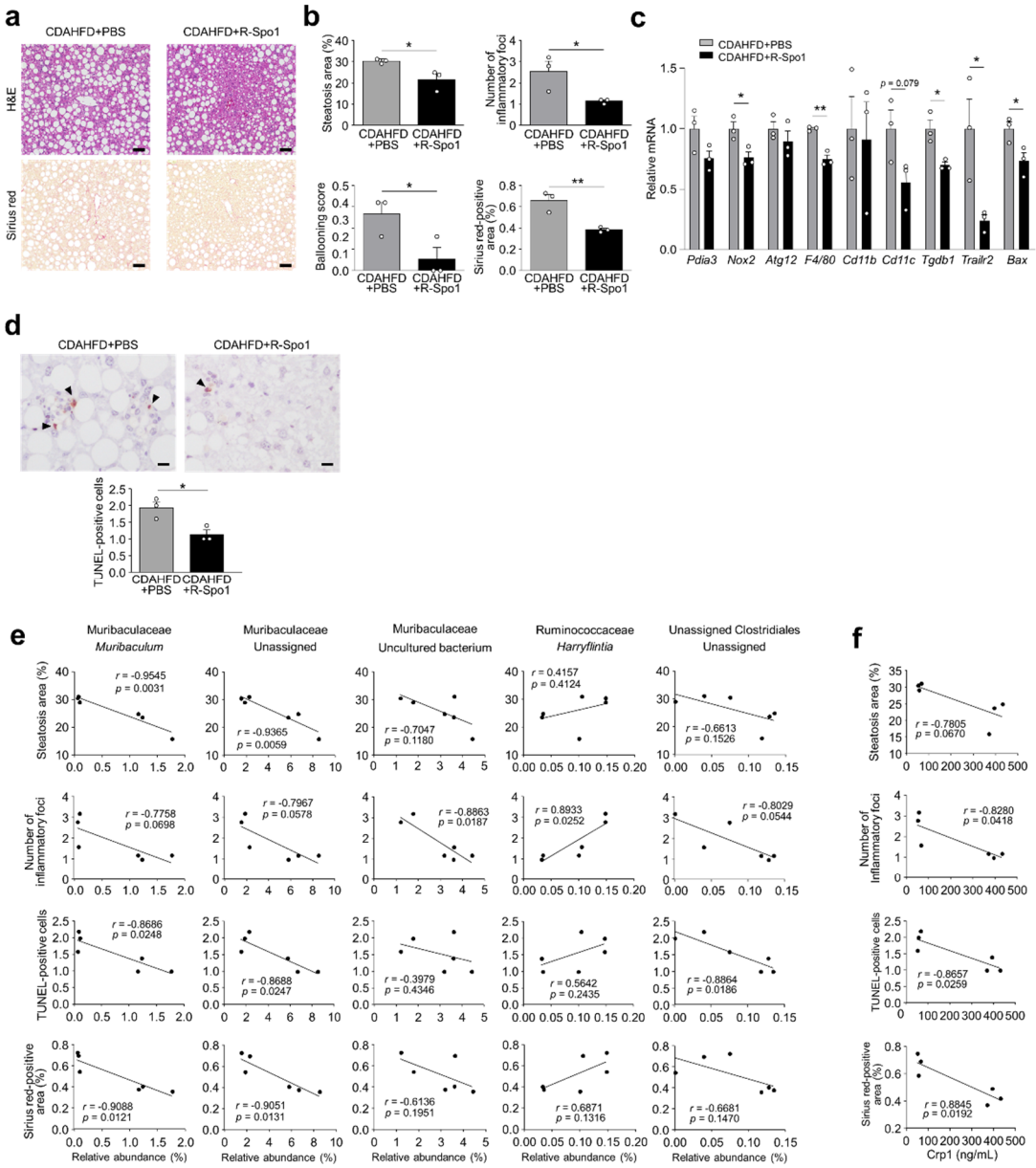


**Figure 11. Restoration of α-defensin by R-Spo1 administration improves NASH progression by suppressing dysbiosis.**

(a) Representative images of H&E- and Sirius red-stained liver sections. Scale bars: 50 μm. (b) Quantification of steatosis area, the number of inflammatory foci and Sirius red-positive area. (c) Hepatic mRNA expression of ER stress, oxidative stress, autophagy, inflammation, and apoptosis marker genes. (d) Representative images of TUNEL staining of liver sections (upper). Scale bars: 10

μm. Quantification of TUNEL-positive cells (lower). (e) Correlation analysis between relative abundance of individual genera and NASH pathology. (f) Correlation analysis between fecal Crp1 levels and NASH pathology. Data are shown as mean ± SEM for $n = 3$ per group. *$P < 0.05$ and **P < 0.01 by unpaired 2-tailed Student's t test (b–d) and Pearson correlation test (e and f).

### 3.4 Oral administration of α-defensin suppresses dysbiosis and ameliorates NASH pathology

Finally, since granules of Paneth cells contain microbicidal components in addition to abundant α-defensins[51], we investigated whether oral administration of an exogenous α-defensin prevents dysbiosis and subsequent NASH development. Crp4 has the most potent in vitro bactericidal activities among Crps[52], and oral administration of Crp4 improved the homeostasis of the intestinal microbiota in GVHD model and in a chronic social defeat stress model[35,53]. Therefore, Crp4 was administered orally to CDAHFD-fed mice for 6 wk. Because C57BL/6 strain lacks the Crp4 gene[54] and dosing with Crp4 introduces an exogenous α-defensin, we confirmed that orally administered Crp4 reached the intestinal lumen by measuring levels of fecal Crp4 (Fig. 12a). To assess whether oral Crp4 suppressed dysbiosis, the intestinal microbiota composition was analyzed. At the family level, among the intestinal bacteria that increased in the CDAHFD group during disease progression, the proportion of Eggerthellaceae, Streptococcaceae, and Ruminococcaceae decreased with Crp4 administration (Fig. 12b). At the genus level, the outgrowth of *Harryflintia* was inhibited by Crp4 administration comparably to R-Spo1 treatment. On the other hand, the increase of uncultured Lachnospiraceae and *Ruminoclostridium 9*, which were not reversed by R-Spo1 treatment decreased with Crp4 administration (Fig. 12c). These results indicated that oral administration of α-defensin suppressed

dysbiosis related to NASH, correcting abnormal proportion of the intestinal bacteria partially different from R-Spo1 administration.

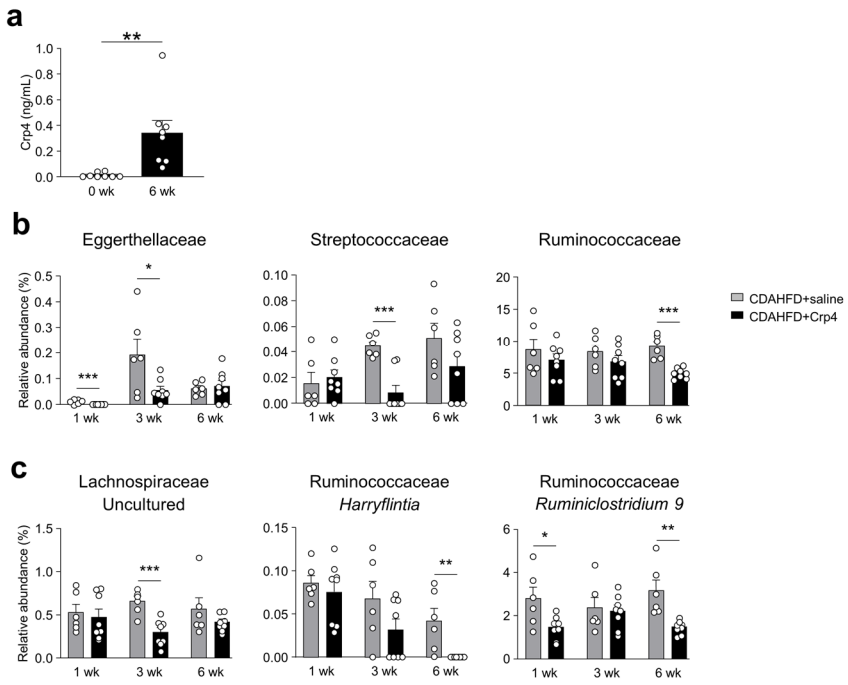


**Figure 12. Oral administration of Crp4 suppresses dysbiosis.**

Six-week-old C57BL6J mice were fed with CDAHFD to induce NASH and orally administered with Crp4 at a dose of 110 μg twice daily for 6 wk. (a) Fecal levels of Crp4 in CDAHFD+Crp4 group were analyzed by sandwich ELISA at 0 and 6 wk. (b) Relative abundance of individual genera at family level that were significantly recovered in CDAHFD+Crp4 group from CDAHFD group of 13 family in Fig. 3c. (c) Relative abundance of individual genera at genus level that were significantly recovered in CDAHFD+Crp4 group from CDAHFD group of 28 genera shown in Fig. 3d. Data are shown as mean ± SEM for $n$ = 6–8 per group. *$P$ < 0.05, **$P$ < 0.01 and ***$P$ < 0.001, by unpaired 2-tailed Student's t test.

To assess whether oral administration of Crp4 ameliorated liver fibrosis by suppressing dysbiosis, histological analysis of liver was performed. The number of inflammatory foci, hepatocellular ballooning, and the area of fibrosis significantly decreased by oral administration of Crp4, even though the area of hepatic steatosis was not affected (Fig. 13, a and b). Analysis of liver gene expression revealed that Crp4 administration increased *Atg12* mRNA levels, decreased *Cd11b* and *Tgfb1* mRNAs, and tended to decrease levels of *Nox2* and *Cd11c* mRNAs. Genes that decreased in expression by R-Spo1 treatment including *F4/80*, *Trailr2*, and *Bax* were unaffected by oral Crp4 administration (Fig. 13c). TUNEL-positive cells in the liver decreased significantly in the Crp4-treated mice compared to untreated CDAHFD-fed mice (Fig. 13d). Moreover, both *Harryflintia* and *Ruminiclostridium 9*, which decreased by Crp4 administration, were positively correlated with the number of inflammatory foci and TUNEL-positive cells, showing that Crp4 ameliorated inflammation and apoptosis followed by fibrosis in the liver via suppressing dysbiosis (Fig. 13e).

Taken together, R-Spo1 and Crp4 prevented liver fibrosis with ameliorating inflammation and apoptosis via suppressing dysbiosis, though, the gene expression in the liver and the intestinal microbiota, which improved by Crp4 administration, were different from those by R-Spo1 treatment, suggesting different underlying mechanism.

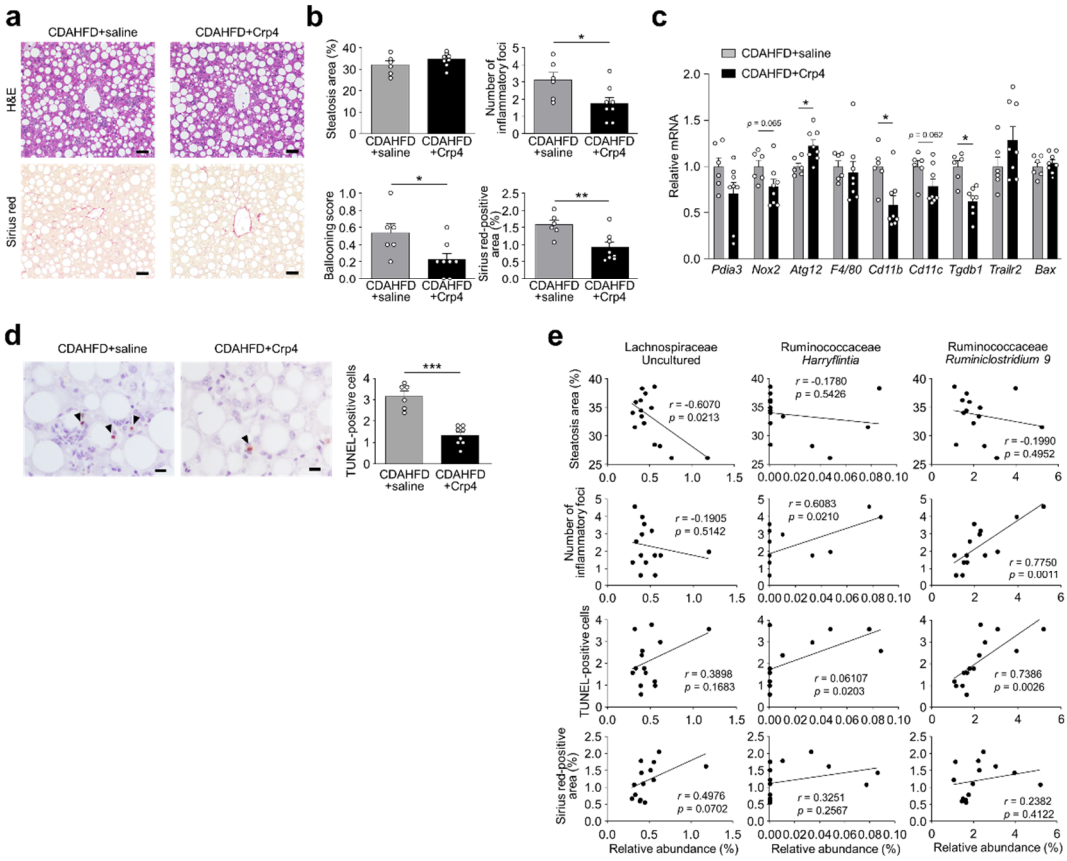


**Figure 13. Oral administration of α-defensin increases autophagy related gene expression and ameliorates liver fibrosis by suppressing dysbiosis.**

(a) Representative images of H&E- and Sirius red-stained liver sections. Scale bars: 50 μm. (b) Quantification of steatosis area, the number of inflammatory foci and Sirius red-positive area. (c) Hepatic mRNA expression of ER stress, oxidative stress, autophagy, inflammation, and apoptosis marker genes. (d) Representative images of TUNEL staining of liver sections (left). Scale bars: 10 μm. Quantification of TUNEL-positive cells (right). (e) Correlation analysis between relative abundance of individual genera and NASH pathology. Data are shown as mean ± SEM for $n$ = 6–8 per group. *$P$ < 0.05, **$P$ < 0.01 and ***$P$ < 0.001, by unpaired 2-tailed Student's t test (b, c, d) and Pearson correlation test (e).

## Chapter 4. Discussion

### 4.1 Relationship between Paneth cell α-defensin and dysbiosis associated with NASH

NASH is one of the largest urgent unmet medical needs with continuously increasing numbers of patients worldwide. Recently, fibrosis was shown to be the major determinant of mortality in patients with NASH, so that understanding the mechanisms of fibrosis development in NASH is extremely important[3,55,56]. This study focused on undetermined mechanisms of the "gut-liver axis" that lead to liver fibrosis in NASH pathology and analyzed the relationship between Paneth cell α-defensins and NASH pathology via dysbiosis. Although high-fat diet (HFD) induces NAFLD, HFD itself generally does not induce severe NASH pathology with fibrosis in mouse models[57]. Therefore, we chose CDAHFD-induced mouse model of NASH, which have been reported to induce progressive liver fibrosis with acceleration of fat accumulation in the liver[58]. In this study, CDAHFD model showed hepatic inflammation and apoptosis accompanied by ER stress, oxidative stress, and impairment autophagy in the liver during disease progression resemble to NASH patient[7]. Furthermore, we have clarified that the CDAHFD group exhibits dysbiosis, sharing some similar features with NAFLD/NASH patients. α-Diversity of the intestinal microbiota decreased in the CDAHFD group consistent with the previous report[59]. At the family level, Prevotellaceae, reported to increase in NAFLD patients[17], was elevated in the CDAHFD group. At the genus level, *Bacteroides*, known to increase in NASH patients and positively correlated with fibrosis score[60], was also elevated in the CDAHFD group. These results suggested that CDAHFD model is a suitable model for analyzing the relationship between NASH pathology and the intestinal homeostasis.

Dysbiosis has been reported to occur in NASH patients, but the cause of dysbiosis has not been well understood because the composition of the intestinal microbiota is affected by varied factors including diet, environmental factors, and host-derived factors[61]. In this study, Crp1, an abundant mouse α-

defensin, significantly decreased before NASH onset along with disease progression and increased α-defensin levels by R-Spo1 administration suppressed dysbiosis and ameliorated steatosis, inflammation, apoptosis, and fibrosis in the liver. R-Spo1 enhanced luminal secretion of α-defensin by regeneration of Paneth cells, though, Paneth cells secrete other antimicrobial proteins including lysozyme and secretory phospholipase A2[62]. In addition, R-Spo1 is reported to increase not only numbers of Paneth cells but also goblet cells[35] secreting mucus, which harbors the intestinal microbiota and influence its composition[63]. Therefore, we further tested whether oral administration of α-defensin prevents NASH, and oral administration of Crp4 suppressed dysbiosis and attenuated NASH pathology. These results indicated that reduction of α-defensin caused dysbiosis and further promoted the development of NASH.

Because secretion of misfolded reduced-form α-defensin from abnormal Paneth cells has been reported to be related to dysbiosis in Crohn's disease model mice[53], whether rCrp1 is secreted in CDAHFD-fed mice was investigated. rCrp1 was not observed in the CDAHFD group, indicating that not abnormal quality but decreased quantity of α-defensin is involved.

### 4.2 Involvement of Paneth cell α-defensin in NASH pathology through regulation of the intestinal microbiota

While both R-Spo1 and Crp4 inhibited the outgrowth of *Harryflintia*, reported to be increased in the animal model of hyperlipidemia and atherosclerosis[64], they affected the intestinal microbiota differently, i.e., R-Spo1 restored Muribaculaceae, whereas Crp4 inhibited the outrgrowth of *Ruminiclostridium 9*. The composition and function of the intestinal microbiota differ between the mucus side and the luminal side in the intestine, forming a unique ecosystem[65]. Muribaculaceae is known as the mucus-resident commensal bacteria[66], while *Ruminiclostridium 9* is reported to be a characteristic luminal bacteria[67]. It is considered that secreted antimicrobial peptides including α-

defensin, do not easily diffuse into the intestinal lumen but are trapped in the mucus layer[68]. Furthermore, human Paneth cell α-defensin HD5 does not elicit bactericidal activities against Muribaculaceae, suggesting a promotion of colonization[31]. Therefore, it is possible that intravenously administered R-Spo1 enhanced α-defensin secretion from *de novo* Paneth cells into mucus layer and predominantly contributed to modifying mucosa-associated bacteria including Muribaculaceae. In contrast to R-Spo1, orally administered α-defensin is expected to diffuse into the intestinal lumen. Thus, it is considered that orally administrated Crp4 mainly affected luminal resident bacteria including *Ruminiclostridium 9*. These findings provide an insight that R-Spo1 and Crp4 modified bacteria localized in mucus and lumen, respectively.

Although both R-Spo1 and Crp4 administration improved hepatic inflammation and fibrosis, R-Spo1 ameliorated steatosis and decreased apoptosis associated genes including *Trail2* and *Bax*, whereas Crp4 increased expression of *Atg12*, an autophagy related protein. Because various metabolites produced by intestinal bacteria, such as SCFA and bile acids, are known to be involved in NASH pathogenesis[16], it is possible that each intestinal bacteria affects by different mechanisms.

Muribaculaceae, which increased by R-Spo1 treatment, is required for inner mucus layer formation of the intestine and SCFA production, known to have beneficial effects on the host[69,70]. It has been reported that SCFA supplementation improved high fat diet-induced steatosis in liver with reduction of fatty acid transporter and improving lipid metabolism[71]. The expression of *Trailr2*, which decreased by R-Spo1 treatment, has been reported to be increased by free fatty acids in hepatocyte[72]. Therefore, it is suggested that R-Spo1 prevented steatosis, apoptosis, and fibrosis with increasing proportion of Muribacluaceae possibly accompanied by increasing SCFA production.

On the other hand, *Ruminiclostridium 9*, decreased by Crp4 administration in this study, increases in a high-fat/high-fructose diet-induced dyslipidemia model[73]. In addition, *Ruminiclostridium 9* was positively correlated with the number of inflammatory foci in this study, suggesting *Ruminiclostridium*

*9* is deleterious microbiota. *Atg12* whose gene expression increased by Crp4 has a crucial role for autophagy[74], and loss of autophagy in hepatocytes causes apoptosis, inflammation, and fibrosis in the liver[75]. These findings suggested that oral administration of Crp4 prevented liver fibrosis by inhibition of apoptosis induced by impairment of autophagy and inflammation along with inhibiting bacterial outgrowth of *Ruminiclostridium 9*, which is a different mechanism of action from R-Spo1 treatment. Taken together, the different pathological features between R-Spo1 and Crp4 may be related to the difference in the improved intestinal microbiota composition, suggesting that α-defensin is involved in NASH pathology by regulating bacteria affecting liver function in both intestinal mucus and lumen.

### 4.3 Functional alterations of Paneth cells in NASH

Paneth cells regulate the composition of the intestinal microbiota by secreting granules rich in α-defensins in response to cholinergic agents, bacteria, bacterial antigen, and certain dietary factors[26,27,76]. Secretory responses of Paneth cells need a biphasic increase in cytosolic $Ca^{2+}$ concentration, and $Ca^{2+}$-activated potassium channel KCNN4 is the essential modulator of $Ca^{2+}$ concentration during Paneth cell secretion[77]. Mice having defective cystic fibrosis transmembrane conductance regulator (CFTR) show unusual accumulation of Paneth cell granules in the intestinal crypt lumen, suggesting that CFTR is important for dissolution of secreted granules[78]. In this study, the RNA-seq analysis of Paneth cells revealed that the expression of both *KCNN4* and *CFTR* decreased in Paneth cells of the CDAHFD group, suggesting that influx of ions such as $Ca^{2+}$ is impaired. RAS-related GTP-binding protein (Rab) and soluble NSF attachment protein receptor (SNARE) family proteins, which allow vesicle transport and fusion, have key roles in granule secretion. The expression of *Rab26*, which has been reported to localize on secretory granules and required to amylase release in parotid acinar cells[79]. Similarly, vesicle-associated membrane protein 2 (VAMP2) has an essential role for glucagon-like peptide 1 (GLP-1) secretion in intestinal L cell[80]. Paneth cell in the CDAHFD group showed decreased

expression of *Rab26* and *Vamp2*, which are essential for granule secretion. On the other hand, syntaxin-binding protein 1 (Stxbp1), whose overexpression inhibits the SNARE complex assembly and decreases insulin secretion[81], increased in the CDAHFD group. Furthermore, decreased granule secretory function in the CDAHFD group was directly revealed by visualization and quantification of granule secretory response in enteroids. Because mutation of autophagy related genes such as *Atg16L1* leads to the abnormal morphology of Paneth cell granules, autophagy elicits important roles in granule formation and secretion of Paneth cells[82]. It has been reported that *Optn*, which decreased in the CDAHFD group Paneth cells, promotes autophagosome formation via recruitment of Atg12-5-16L1 complex[83]. Our findings that Paneth cells in CDAHFD group showed reduction of *Optn* expression suggests that abrogation of autophagy leads to abnormal granule formation and decreased granule secretion. Taken together, it is possible that decreased granule secretion in mice fed CDAHFD occurs through impairment of influx of ions such as $Ca^{2+}$, vesicle transport, and autophagy process in Paneth cells.

### 4.4 Potential prevention and treatment of NASH targeting Paneth cell α-defensin

There are currently no approved drugs to treat NASH, and the basis of all therapeutic interventions is lifestyle changes including diet and exercise[2]. This study showed the possibility that decrease of Paneth cell α-defensin secretion could be the cause of onset and the progression of NASH via dysbiosis. The relationship between diet and Paneth cell function has been reported. Leucine, a dietary factor, and butyrate, generated by the metabolism of dietary fiber by the intestinal bacteria, induce the secretion of α-defensin from Paneth cell[76]. N-3 polyunsaturated fatty acids increased expression of antimicrobial peptides, including α-defensin, and ameliorated intestine atrophy in total parental nutrition model mice[84]. In addition, lactate increases expansion of Paneth cells by enhancing wnt signaling[85], which is expected to increase α-defensin secretion. These findings suggest that dietary

intervention targeting Paneth cell α-defensin could be a novel method of NASH prevention and treatment.

Although CDAHFD model mice has limitations such as not showing obesity and insulin resistance usually observed in patients with NASH[86], our findings provide novel insights into the process of NASH fibrosis in the "gut-liver axis" and possibly propose a novel therapeutic approach for NASH via regulation of the intestinal microbiota targeting Paneth cell α-defensin.

## Chapter 5. Conclusion

This study revealed that decrease of Paneth α-defensin secretion associated with impairment of granule secretory function exacerbated liver apoptosis and inflammation via dysbiosis, contributing to development of NASH fibrosis. Both stimulating differentiation of Paneth cells to increase α-defensin secretion by R-Spo1 and oral administration of α-defensin improved dysbiosis and prevented fibrosis. Taken together, our findings provide novel insights into NASH pathophysiology in the "gut-liver axis" and further propose a novel therapeutic approach for NASH targeting Paneth cell α-defensin via regulation of the intestinal microbiota.

**References**


1. Chalasani, N. *et al.* The diagnosis and management of nonalcoholic fatty liver disease: Practice guidance from the American Association for the Study of Liver Diseases. *Hepatology* **67**, 328–357 (2018).
2. Younossi, Z. *et al.* Global perspectives on nonalcoholic fatty liver disease and nonalcoholic steatohepatitis. Hepatology 69, 2672–2682 (2019).
3. Dulai, P. S. *et al.* Increased risk of mortality by fibrosis stage in nonalcoholic fatty liver disease: Systematic review and meta-analysis. *Hepatology* **65**, 1557–1565 (2017).
4. Christ, A., Lauterbach, M. & Latz, E. Western diet and the immune system: An inflammatory connection. *Immunity* **51**, 794–811 (2019).
5. Williams, C. D. *et al.* Prevalence of nonalcoholic fatty liver disease and nonalcoholic steatohepatitis among a largely middle-aged population utilizing ultrasound and liver biopsy: A prospective study. *Gastroenterology* **140**, 124–131 (2011).
6. McPherson, S. *et al.* Evidence of NAFLD progression from steatosis to fibrosing-steatohepatitis using paired biopsies: Implications for prognosis and clinical management. *J. Hepatol.* **62**, 1148–1155 (2015).
7. Arab, J. P., Arrese, M. & Trauner, M. Recent Insights into the Pathogenesis of Nonalcoholic Fatty Liver Disease. *Annu. Rev. Pathol. Mech. Dis.* **13**, 321–350 (2018).
8. Marchesini, G., Petta, S. & Grave, R. D. Diet, weight loss, and liver health in nonalcoholic fatty liver disease: pathophysiology, evidence, and practice. *Hepatology* 63, 2032–2043 (2016).
9. Parthasarathy, G., Revelo, X. & Malhi, H. Pathogenesis of Nonalcoholic Steatohepatitis: An Overview. *Hepatol. Commun.* **4**, 478–492 (2020).
10. Cani, P. D. *et al*. Microbial regulation of organismal energy homeostasis. *Nat. Metab.* **1**, 34–

46 (2019).

11. Levy, M., Kolodziejczyk, A. A., Thaiss, C. A. & Elinav, E. Dysbiosis and the immune system. *Nat. Rev. Immunol.* **17**, 219–232 (2017).

12. Bäckhed F, *et al*. The gut microbiota as an environmental factor that regulates fat storage. *Proc. Natl. Acad. Sci. USA* **101**, 15718–15723 (2004).

13. Ley, R. E., Turnbaugh, P. J., Klein, S. & Gordon, J. I. Human gut microbes associated with obesity SI. *Nature* **444**, 1022–1023 (2006).

14. Tripathi, A. *et al.* The gut-liver axis and the intersection with the microbiome. *Nat. Rev. Gastroenterol. Hepatol.* **15**, 397–411 (2018).

15. Zmora, N., Suez, J. & Elinav, E. You are what you eat: diet, health and the gut microbiota. *Nat. Rev. Gastroenterol. Hepatol.* **16**, 35–56 (2019).

16. Kolodziejczyk, A. A., Zheng, D., Shibolet, O. & Elinav, E. The role of the microbiome in NAFLD and NASH. *EMBO Mol. Med.* **11**, 1–13 (2019).

17. Zhu, L. *et al.* Characterization of gut microbiomes in nonalcoholic steatohepatitis (NASH) patients: A connection between endogenous alcohol and NASH. *Hepatology* **57**, 601–609 (2013).

18. Mouzaki, M. *et al.* Intestinal microbiota in patients with nonalcoholic fatty liver disease. *Hepatology* **58**, 120–127 (2013).

19. Loomba, R. *et al.* Gut Microbiome-Based Metagenomic Signature for Non-invasive Detection of Advanced Fibrosis in Human Nonalcoholic Fatty Liver Disease. *Cell Metab.* **25**, 1054-1062.e5 (2017).

20. Krishnan, S. *et al.* Gut Microbiota-Derived Tryptophan Metabolites Modulate Inflammatory Response in Hepatocytes and Macrophages. *Cell Rep.* **23**, 1099–1111 (2018).

21. Henao-Mejia, J. *et al.* Inflammasome-mediated dysbiosis regulates progression of NAFLD

and obesity. *Nature* **482**, 179–185 (2012).

22. Allaire, J. M. *et al.* The intestinal epithelium: Central coordinator of mucosal immunity. *Trends Immunol.* **39**, 677–696 (2018).

23. Ouellette, A. J. *et al.* Developmental regulation of cryptdin, a corticostatin/defensin precursor mRNA in mouse small intestinal crypt epithelium. *J. Cell Biol.* **108**, 1687–1695 (1989).

24. Jones, D. E. & Bevins, C. L. Paneth cells of the human small intestine express an antimicrobial peptide gene. *J. Biol. Chem.* **267**, 23216–23225 (1992).

25. Jones, D. E. & Bevins, C. L. Defensin-6 mRNA in human Paneth cells: implications for antimicrobia peptides in host defense of the human bowel. *FEBS Lett.* **315**, 187–192 (1993).

26. Ayabe, T. et al. Secretion of microbicidal α-defensins by intestinal Paneth cells in response to bacteria. *Nat. Immunol.* **1**, 113–118 (2000).

27. Yokoi, Y. *et al.* Paneth cell granule dynamics on secretory responses to bacterial stimuli in enteroids. *Sci. Rep.* **9**, 2710 (2019).

28. Masuda, K., Sakai, N., Nakamura, K., Yoshioka, S. & Ayabe, T. Bactericidal activity of mouse α-defensin cryptdin-4 predominantly affects noncommensal bacteria. *J. Innate Immun.* **3**, 315–326 (2011).

29. Wilson, C. L. *et al.* Regulation of intestinal alpha-defensin activation by the metalloproteinase matrilysin in innate host defense. *Science* **286**, 113–117 (1999).

30. Salzman, N. H. *et al.* Enteric defensins are essential regulators of intestinal microbial ecology. *Nat. Immunol.* **11**, 76–83 (2010).

31. Ou, J., Liang, S., Guo, X. K. & Hu, X. α-Defensins promote bacteroides colonization on mucosal reservoir to prevent antibiotic-induced dysbiosis. *Front. Immunol.* **11**, 2065 (2020).

32. Cadwell, K. *et al.* A key role for autophagy and the autophagy gene Atg16l1 in mouse and human intestinal Paneth cells. *Nature* **456**, 259–263 (2008).

33. Eriguchi, Y. *et al.* Graft-versus-host disease disrupts intestinal microbial ecology by inhibiting Paneth cell production of α-defensins. *Blood* **120**, 223–232 (2012).

34. Eriguchi, Y. *et al.* Decreased secretion of Paneth cell α-defensins in graft-versus-host disease. *Transpl. Infect. Dis.* **17**, 702–706 (2015).

35. Hayase, E. *et al*. R-Spondin1 expands Paneth cells and prevents dysbiosis induced by graft-versus-host disease. *J. Exp. Med.* **214**, 3507–3518 (2017).

36. Hodin, C. M. *et al.* Reduced Paneth cell antimicrobial protein levels correlate with activation of the unfolded protein response in the gut of obese individuals. *J. Pathol.* **225**, 276–284 (2011).

37. Nakamura, K., Sakuragi, N., Takakuwa, A. & Ayabe, T. Paneth cell α-defensins and enteric microbiota in health and disease. *Biosci. Microbiota Food Health* **35**, 57–67 (2016).

38. Herlemann, D. P. R. *et al.* Transitions in bacterial communities along the 2000 km salinity gradient of the Baltic Sea. *ISME J.* **5**, 1571–1579 (2011).

39. Bolyen, E. *et al.* Reproducible, interactive, scalable and extensible microbiome data science using QIIME 2. *Nat. Biotechnol.* **37**, 852–857 (2019).

40. Callahan, B. J. *et al.* DADA2: High-resolution sample inference from Illumina amplicon data. *Nat. Methods* **13**, 581–583 (2016).

41. Price, M. N., Dehal, P. S. & Arkin, A. P. FastTree 2 - Approximately maximum-likelihood trees for large alignments. *PLoS One* **5**, (2010).

42. Katoh, K. & Standley, D. M. MAFFT multiple sequence alignment software version 7: Improvements in performance and usability. *Mol. Biol. Evol.* **30**, 772–780 (2013).

43. Nakamura, K., Sakuragi, N. & Ayabe, T. A monoclonal antibody-based sandwich enzyme-linked immunosorbent assay for detection of secreted α-defensin. *Anal. Biochem.* **443**, 124–131 (2013).

44. Yokoi, Y., Adachi, T., Sugimoto, R., Kikuchi, M. & Ayabe, T. Biochemical and Biophysical Research Communications Simultaneous real-time analysis of Paneth cell and intestinal stem cell response to interferon- g by a novel stem cell niche tracking method. *Biochem. Biophys. Res. Commun.* **545**, 14–19 (2021).

45. Shimizu, Y. *et al*. Paneth cell α-defensin misfolding correlates with dysbiosis and ileitis in Crohn's disease model mice. *Life Sci. Alliance* **3**, e201900592 (2020).

46. Kim, K. *et al.* Mitogenic Influence of Human R-Spondin1 on the Intestinal Epithelium. **309**, 1256–1260 (2005).

47. Takashima, S. *et al.* The Wnt agonist R-spondin1 regulates systemic graft-versus-host disease by protecting intestinal stem cells. *J. Exp. Med.* **208**, 285–294 (2011).

48. Tomisawa, S. *et al*. Efficient production of a correctly folded mouse α-defensin, cryptdin-4, by refolding during inclusion body solubilization. *Protein. Expr. Purif.* **112**, 21–28 (2015).

49. Fasano, A. *et al.* Zonulin, a newly discovered modulator of intestinal permeability, and its expression in coeliac disease. *Lancet* **355**, 1518–1519 (2000).

50. Selsted, M. E., Miller, S. I., Henschen, A. H. & Ouellette, A. J. Enteric defensins: Antibiotic peptide components of intestinal host defense. *J. Cell Biol.* **118**, 929–936 (1992).

51. Wehkamp, J. & Stange, E. F. An Update Review on the Paneth Cell as Key to Ileal Crohn's Disease. *Front. Immunol.* **11**, (2020).

52. Ouellette, A. J. *et al.* Mouse Paneth cell defensins: Primary structures and antibacterial activities of numerous cryptdin isoforms. *Infect. Immun.* **62**, 5040–5047 (1994).

53. Suzuki, K. et al. Decrease of α-defensin impairs intestinal metabolite homeostasis via dysbiosis in mouse chronic social defeat stress model. *Sci. Rep.* **11**, 9915 (2021).

54. Shanahan, M. T., Tanabe, H. & Ouellette, A. J. Strain-specific polymorphisms in paneth cell α-defensins of C57BL/6 mice and evidence of vestigial myeloid α-defensin pseudogenes.

*Infect. Immun.* **79**, 459–573 (2011).

55. Angulo, P. *et al.* Liver fibrosis, but no other histologic features, is associated with long-term outcomes of patients with nonalcoholic fatty liver disease. *Gastroenterology* **149**, 389-397.e10 (2015).

56. Younossi, Z. M. *et al.* Nonalcoholic steatofibrosis independently predicts mortality in nonalcoholic fatty liver disease. *Hepatol. Commun.* **1**, 421–428 (2017).

57. Charlton, M. *et al.* Fast food diet mouse: novel small animal model of NASH with ballooning, progressive fibrosis, and high physiological fidelity to the human condition. *AJP Gastrointest. Liver Physiol.* **301**, G825–G834 (2011).

58. Matsumoto, M. *et al.* An improved mouse model that rapidly develops fibrosis in non-alcoholic steatohepatitis. *Int. J. Exp. Pathol.* **94**, 93–103 (2013).

59. Del Chierico, F. *et al.* Gut microbiota profiling of pediatric nonalcoholic fatty liver disease and obese patients unveiled by an integrated meta-omics-based approach. *Hepatology* **65**, 451–464 (2017).

60. Boursier, J. *et al.* The severity of nonalcoholic fatty liver disease is associated with gut dysbiosis and shift in the metabolic function of the gut microbiota. *Hepatology* **63**, 764–775 (2016).

61. Schmidt, T. S. B., Raes, J. & Bork, P. The Human Gut Microbiome: From Association to Modulation. *Cell* **172**, 1198–1215 (2018).

62. Ouellette, A. J. Paneth cell α-defensins in enteric innate immunity. *Cell. Mol. Life Sci.* **68**, 2215–2229 (2011).

63. Sicard, J. F., Bihan, G. Le, Vogeleer, P., Jacques, M. & Harel, J. Interactions of intestinal bacteria with components of the intestinal mucus. *Front. Cell. Infect. Microbiol.* **7**, 387 (2017).

64. Jiang, T. *et al*. Lactobacillus Mucosae strain promoted by a high-fiber diet in genetic obese child alleviates lipid metabolism and modifies gut microbiota in ApoE-/- mice on a western diet. *Microorganisms* **8**, 1225 (2020).

65. Ringel, Y. *et al*. High throughput sequencing reveals distinct microbial populations within the mucosal and luminal niches in healthy individuals. *Gut Microbes* **6**, 173–181 (2015).

66. Pereira, F. C. *et al.* Rational design of a microbial consortium of mucosal sugar utilizers reduces Clostridiodes difficile colonization. *Nat. Commun.* **11**, 5104 (2020).

67. Wu, M. *et al*. The Differences between luminal microbiota and mucosal microbiota in mice. *J. Microbiol. Biotechnol.* **30**, 287–295 (2020).

68. Meyer-Hoffert, U. *et al.* Secreted enteric antimicrobial activity localises to the mucus surface layer. *Gut* **57**, 764–771 (2008).

69. Smith, B. J. *et al*. Changes in the gut microbiota and fermentation products associated with enhanced longevity in acarbose-treated mice. *BMC Microbiol.* **19**, 130 (2018)

70. Volk, J. K. *et al.* The Nlrp6 inflammasome is not required for baseline colonic inner mucus layer formation or function. *J. Exp. Med.* **216**, 2602–2618 (2019).

71. Weitkunat, K. *et al.* Short-chain fatty acids and inulin, but not guar gum, prevent diet-induced obesity and insulin resistance through differential mechanisms in mice. *Sci. Rep.* **7**, 1–13 (2017).

72. Cazanave, S. C. *et al.* Death receptor 5 signaling promotes hepatocyte lipoapoptosis. *J. Biol. Chem.* **286**, 39336–39348 (2011).

73. Horne, R. G. *et al.* High fat-high fructose diet-induced changes in the gut microbiota associated with dyslipidemia in Syrian hamsters. *Nutrients* **12**, 1–20 (2020).

74. Hanada, T. *et al.* The Atg12-Atg5 conjugate has a novel E3-like activity for protein lipidation in autophagy. *J. Biol. Chem.* **282**, 37298–37302 (2007).

75. Ni, H. *et al.* Nrf2 promotes the development of fibrosis and tumorigenesis in mice with defective hepatic autophagy. *J. Hepatol.* **61**, 617–625 (2014).

76. Takakuwa, A. *et al*. Butyric acid and leucine induce α-defensin secretion from small intestinal Paneth cells. *Nutrients* **11**, 2817 (2019).

77. Ayabe, T. *et al.* Modulation of mouse paneth cell α-defensin secretion by mIKCa1, a Ca2+-activated, intermediate conductance potassium channel. *J. Biol. Chem.* **277**, 3793–3800 (2002).

78. Clarke, L. L. *et al*. Abnormal Paneth cell granule dissolution and compromised resistance to bacterial colonization in the intestine of CF mice. *Am. J. Physiol. Gastrointest. Liver Physiol.* **286**, 1050–1058 (2004).

79. Nashida, T., Imai, A. & Shimomura, H. Relation of Rab26 to the amylase release from rat parotid acinar cells. *Arch. Oral Biol.* **851**, 89–95 (2006).

80. Li, S. K., Zhu, D., Gaisano, H. Y. & Brubaker, P. L. Role of vesicle-associated membrane protein 2 in exocytosis of glucagon-like peptide-1 from the murine intestinal L cell. *Diabetologia* **57**, 809–818 (2014).

81. Dong, Y., Wan, Q., Yang, X., Bai, L. & Xu, P. Interaction of Munc18 and Syntaxin in the regulation of insulin secretion. *Biochem. Biophys. Res. Commun.* **360**, 609–614 (2007).

82. Saitoh, T. *et al.* Loss of the autophagy protein Atg16L1 enhances endotoxin-induced IL-1β production. *Nature* **456**, 264–268 (2008).

83. Bansal, M. *et al.* Optineurin promotes autophagosome formation by recruiting the autophagy-related Atg12-5-16L1 complex to phagophores containing the Wipi2 protein. *J. Biol. Chem.* **293**, 132–147 (2018).

84. Wang, J. *et al.* N-3 polyunsaturated fatty acid-enriched lipid emulsion improves Paneth cell function via the IL-22/Stat3 pathway in a mouse model of total parenteral nutrition. *Biochem.*

*Biophys. Res. Commun.* **490**, 253–259 (2017).

85. Lee, Y. S. *et al.* Microbiota-Derived Lactate Accelerates Intestinal Stem-Cell-Mediated Epithelial Development. *Cell Host Microbe* **24**, (2018).

86. Ulmasov, B. *et al.* An Inhibitor of Arginine-Glycine-Aspartate-Binding Integrins Reverses Fibrosis in a Mouse Model of Nonalcoholic Steatohepatitis. *Hepatol. Commun.* **3**, 246–261 (2019).

**Acknowledgements**

I am grateful to many people who supported me, so that I was able to start my doctoral study and continue my all research. First of all, I would like to thank the people who strongly supported me.

I would like to express my deepest gratitude to Professor Emeritus Tokiyoshi Ayabe for invaluable advice and guidance throughout all of my research activities. I thank for his great patience and guiding me to the appropriate way to reach my final goal.

I sincerely and deeply appreciate Professor Kiminori Nakamura for teaching me the fundamentals of all experimental methods, ways of thinking, and attitudes toward research. I thank for devoting a great deal of his time, intelligence, and emotional support to me a lot. I also deeply appreciate Assistant Professor Yuki Yokoi and Dr. Yu Shimizu in the Innate Immunity Laboratory for courteous guidance and support throughout my research.

I would like to thank Professor Tomoyasu Aizawa for continuous support of my research as an important collaborator as well as the associate examiner of the thesis. I also thank Associate Professor Ryota Uehara for supporting my research as associate examiner of the thesis. I sincerely appreciate Professor Andre J Ouellette at Kech School of Medicine in University of Southern California for precise advice and constructive discussions. I would like to thank Ms. Aiko Kuroishi and Ms. Mutsuko Tanaka who provided enormous technical support. I thank Ms. Mari Tatsumi who has always helped me in my entire laboratory life. Finally, I gratitude to all the laboratory members for their support in continuing and accomplishing this work.